Modelling and Simulation of Particle-particle Interaction in a Magnetophoretic Bio-Separation Chip

by Manjurul Alam, Bachelor of Engineering

A Thesis Submitted in Partial
Fulfillment of the Requirements
for the Degree of
Master of Science
in the field of Mechanical Engineering

Advisory Committee:

Jeff Darabi, Chair

Terry X. Yan

Soondo Kweon

Graduate School
Southern Illinois University Edwardsville
August, 2016

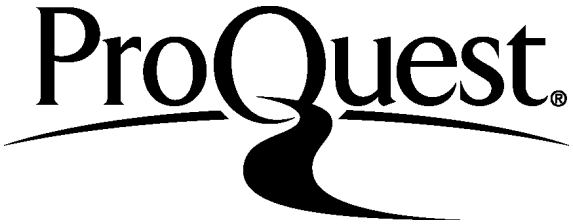

ABSTRACT

MODELLING AND SIMULATION OF PARTICLE-PARTICLE INTERACTION IN A MAGNETOPHORETIC BIO-SEPARATION CHIP

by

Manjurul Alam

Chairperson: Dr. Jeff Darabi

A Lagrangian particle trajectory model is developed to predict the interaction between cell-bead complexes and to track the positions and angles of the particles in a magnetophoretic bio-separation chip. Magnetic flux gradients are simulated in OpenFOAM CFD software and imported to MATLAB to obtain the particle trajectories. A connector vector is introduced to calculate the interaction force between two cell-bead particle complexes as they flow through a microfluidic device. The interaction force calculations are performed for cases where the connector vector is parallel, perpendicular, and at an angle of 45 degrees with the applied magnetic field. The trajectories of the particles are simulated by solving a system of eight ordinary differential equations using the fourth order Runge-Kutta method. The model is then used to study the effects of geometric positions and angles of the connector vector between the particles as well as the bead size, cell size, number of beads per cell, and flow rate on the interaction force and trajectories of the particles.

TABLE OF CONTENTS

LIST OF FIGURES

NOMENCLATURE

μ_0	Permeability of free space (N/A^2)
$\vec{p}_x$	Path increment vector along current x (m)
$\vec{p}_y$	Path increment vector along current y (m)
$\vec{R}$	Vector from circuit path element $\vec{p}_x$ to circuit element $\vec{p}_y$ (m)
$\vec{m}$	Magnetic dipole moment (A/m^2)
$\vec{e}_x$	Distance from dipole center to path increment vector of x (m)
$\vec{e}_y$	Distance from dipole center to path increment vector of y (m)
θ	Angle from x-axis to dipole magnetic moment (°)
$\vec{r}$	Distance between dipole centers (m)
$\vec{F}_{xy}$	Interaction force of dipole x on dipole y (N)
$\vec{m}_1$	Magnetic moment of dipole 1 (A/m^2)
$\vec{m}_2$	Magnetic moment of dipole 2 (A/m^2)
r	Magnitude of connector vector distance $\vec{r}$ (m)
$\vec{F}_{d1}$	Hydrodynamic drag force of cell-bead particle complex 1 (N)
$\vec{F}_{d2}$	Hydrodynamic drag force of cell-bead particle complex 2 (N)
R_{p1}	Radius of cell-bead particle complex 1 (m)
R_{p2}	Radius of cell-bead particle complex 2 (m)
η	Dynamic viscosity of the medium (Pa.s)
$\vec{V}_f$	Fluid velocity inside the microchannel (m/s^2)
$\vec{V}_p$	Velocity of particle complex (m/s^2)
Q	Volumetric flow rate (m^3/s)
h	Channel height (m)
w	Channel width (m)
R_{pe}	Equivalent radius of sphere as same volume as the chain (m)

$\vec{F}_{m1}$	Magnetic force of particle complex 1 (N)
$\vec{F}_{m2}$	Magnetic force of particle complex 2 (N)
$\vec{B}$	Applied magnetic field (T)
ρ_b	Density of magnetic beads (kg/m^3)
V_b	Volume of magnetic beads (m^3)
$\vec{M}_b$	Magnetization of magnetic bead (Am^2/kg)
$\vec{F}_{g1}$	Gravitational force of particle complex 1 (N)
$\vec{F}_{g2}$	Gravitational force of particle complex 2 (N)
g	Acceleration due to gravity (m/s^2)
ρ_p	Density of particle complex (kg/m^3)
ρ_f	Density of fluid (kg/m^3)
m_{p1}	Mass of particle complex 1(Kg)
m_{p2}	Mass of particle complex 2(Kg)

CHAPTER I

INTRODUCTION

Overview

In this study, a transport model has been proposed to predict the trapping length of particle complexes in a magnetophoretic bio-separation chip. Using this model, trajectories of two identical particle complexes are observed to analyze the interaction force between them. A Langrangian model is used for particle modelling and Newton's second law of motion is applied to predict the behavior of the particles. The interaction force between the particles is included by assuming that the particle complexes are point dipoles. In this chapter, a brief overview of the magnetophoretic bio-separation technique is provided and the interaction force pertaining to the transport of particles through the channel is also discussed. This chapter also discusses cells, beads and the formation of particle complexes as they move along the channel.

Microfluidic bio-separation

Microfluidic bio-separation process is one of the widely used techniques to separate specific biological entities such as cells, DNA/RNA, proteins, and bacteria from biological samples. The method includes particular labeling of the anticipated biological particles with magnetic beads followed by isolating the marked entities by the use of magnetic separation devices. Magnetic separation is typically used in Lab-on-a-Chip devices, cell separators, micro-total analysis system(μTAS), or DNA/RNA isolators [1-4]. The target biomaterials are labeled in such a way that their surface receptors have strong affinity for the specific magnetic bead

ligands [5].

Magnetophoretic bio-separation process can be employed using two approaches. One is direct binding and the other is indirect binding. In the direct binding method, specific biomaterials are directly attached to surfaces of the magnetic particles by incubation and mixing. The indirect method requires binding a primary antibody to the target cells before adding the beads. Then, magnetic beads with surface-bound secondary antibodies bind to the primary antibodies on the surface of the biomaterials [6]. The magnetic particles are superparamagnetic, which means they have no magnetic hysteresis. These particles become magnetized in the presence of an external magnetic field, but when the magnetic field is removed, they do not experience any kind of magnetic behavior.

Magnetic micro-particles

In magnetic bio-separation, magnetic micro-particles are used to label target biomaterials for separation [7, 8]. These particles are called beads and consist of iron oxide nanoparticles encapsulated by polymer shells. The outer surface of the beads is coated with a particular antibody to bind to a target antigen. It can be said that there are no other interactions with the nonmatching antigens. A schematic of a typical micro-bead is shown in Fig. 1. The main structure of the bead is a spherical shape of the order of micro size diameter containing iron oxide nanoparticles. In these nanoparticles, the alignment of magnetic moments is formed in such a way that they can shift freely under the influence of an applied magnetic field. The reason for using polymer encapsulation is that it allows micro-particles to coat with target biomaterials [9].

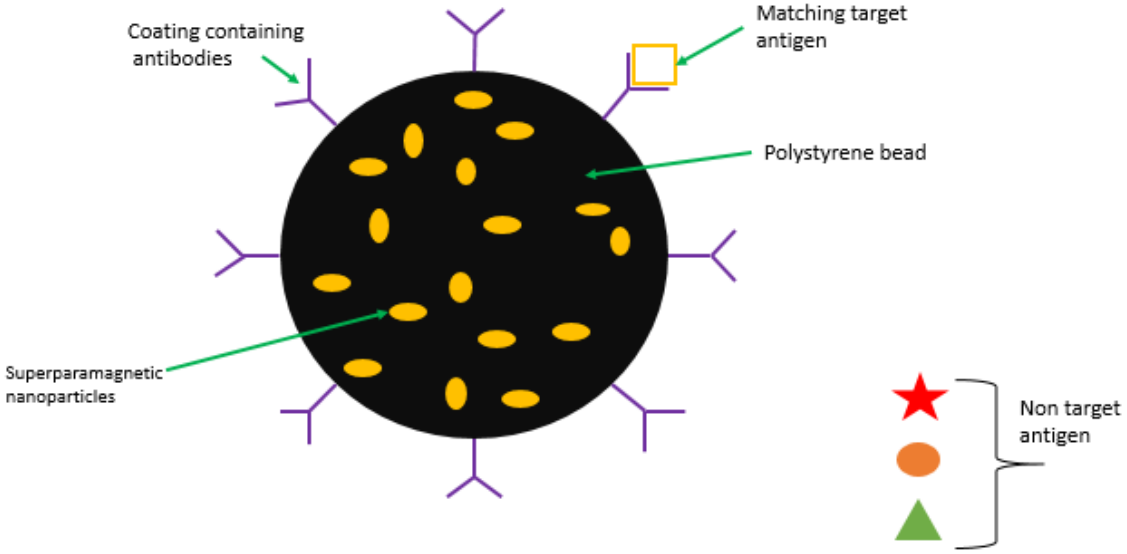

Figure 1: Schematic of a micro-bead used in magnetic bio-separation.

Biomaterials

Magnetic bio-separation is becoming a popular technique to isolate different biological materials. The biological entities can be proteins, DNA/RNA, bacteria, enzymes, cells [10-11]. The isolation of mammalian cells is important in many biomedical and biotechnological applications. Different biomaterials have different sizes. Typically sizes for various biomaterials range from ~10 μm – 100 μm for cells, 20nm – 450 nm for viruses, and 3 nm – 50 nm for proteins [12].

Magnetophoretic bio-separation chip

Magnetic bio-separation is a useful and efficient technique for separating biomaterials. This

method has been largely used in molecular and cell biology over the last few decades [13]. Due to high degree of selectivity between magnetic particles and non-magnetic biomaterials, this separation method is more efficient than conventional bio-separation techniques. A significant number of analytical and experimental studies have been performed in the field of magnetophoretic bio-separation. A model for the magnetophoretic capture of particle in a microfluidic device has been developed by Nandy and Chaudhuri [14]. A magnetophoretic bio-separation chip has been designed, fabricated and modelled by Darabi and Guo [15]. This chip was developed to separate CD4+T cells from blood and was later used to separate DNA from blood [16]. A force analysis on the superparamagnetic bead in a magnetic field was performed by Shevkoplyas and Siegel [17]. Zhu et al. [18] fabricated a magnetic based bio-separation chip using embedded permanent magnets.

Schematic of bio-separation chip

A schematic of a typical magnetophoretic bio-separation chip is shown in Fig. 2. It consists of an inlet port, a buffer solution port, channel, and outlet ports. Solution containing magnetic beads and non-magnetic biomaterials are introduced into the microfluidic channel through inlet ports for the sample and buffer solution. The target cell-bead particle complexes are trapped at the bottom of the channel due to the magnetic force applied by an array of magnets underneath the channel. Non-target biomaterials are not affected by the applied magnetic field and flow to a waste collection tube.

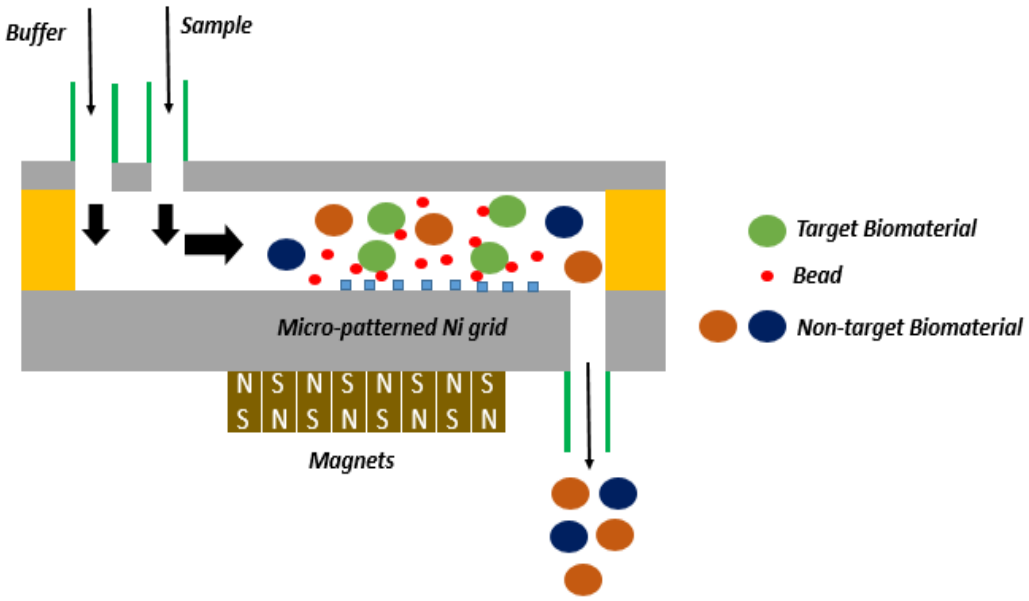

Figure 2: Schematic of a magnetophoretic bio-separation chip.

Cell-bead particle complex

In magnetophoretic bio-separation technique, biomaterials (cells) and magnetic micro-particles form cell-bead particle complex. A schematic of a cell-bead particle complex is shown in Fig. 3. Usually the cell size is larger than the bead size in a magnetic cell separation system. Thus, several micron size beads can bind to the surface of the cell to form a cell-bead complex. Depending on the number of beads attached to cell, the effective mass, volume, density, and radius estimated and used in force calculations during the analysis [19].

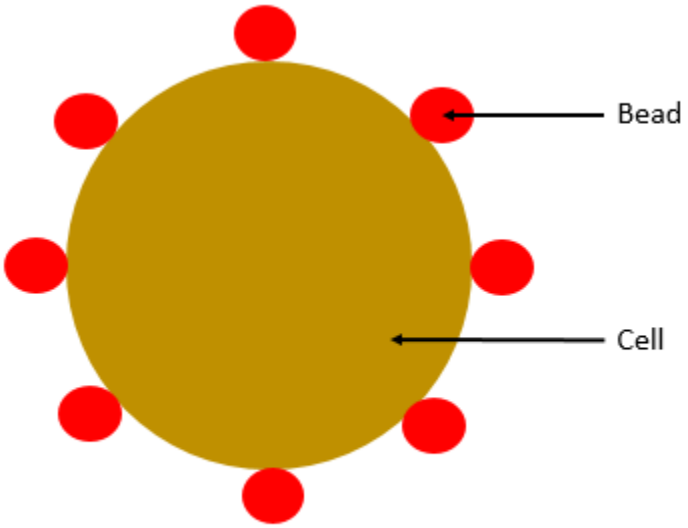

Figure 3: Schematic of a cell-bead particle complex (assuming both cell and bead are spherical in shape). The particle complex consists of core and shell where core (cell) is non-magnetic and shell (beads) is magnetic.

Protein-ligand interaction

A schematic illustration of ligand-receptor binding is shown in Fig. 4. A cell surface has receptors, which cause molecules to undergo metabolic and biological changes in cell. These are transducer proteins, which can bind with an endogenous signaling molecules for conformational change of the protein structure to create cellular response. The cell-surface receptors create bonds to an external ligand molecule which can send an extracellular signal into an intracellular signal. This process is called cell signaling, which can be performed in three steps. These are reception, transduction, and response. When a chemical signal (ligand) bonds to a receptor protein on the cell surface, it changes the protein of the receptor. Then it initiates transduction process and changes molecular pathway of the neighbor molecule. After that the signal triggers a specific cellular response.

There are three kinds of cell-surface receptors and they are G-protein receptors, ion-channel receptors and enzyme-linked protein receptors. G-protein receptors can create bonds with ligands to activate a membrane protein which is called G-protein whereas ion channel receptors bind with a ligand which can open a channel to allow specific ions to pass through the membrane. On the other hand, enzyme-linked receptors have intracellular parts filled with enzyme also can bind with ligands. When a ligand binds to extracellular domain of the receptors, a signal is send to the membrane and activates the enzyme that eventually leads to cellular response. One type of enzyme linked receptor is tyrosine kinase receptor [19-21]. The Neuropilins are a set of surface receptors used in cellular signaling cascades [22].

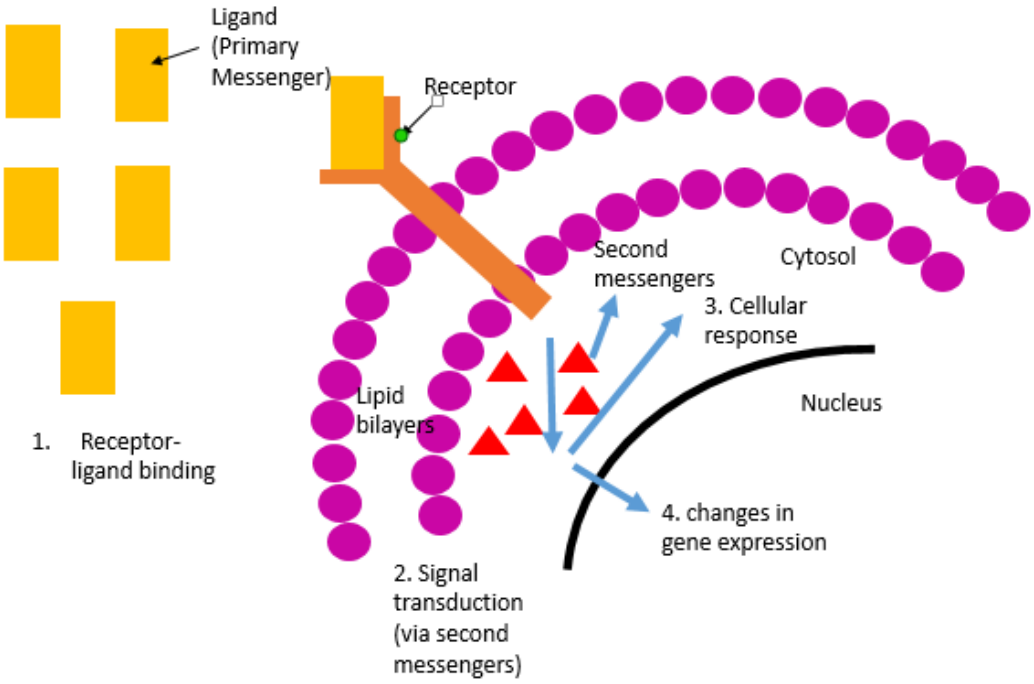

Figure 4: Process of ligand-receptor binding in bio-separation technique

Particle-particle interaction

Particle-particle interaction is possible in two different ways in a magnetophoretic bio-separation chip. One is magnetic interaction force and other is hydrodynamic interaction force between particle complexes [23-25]. In magnetophoretic bio-separation technique, the interaction between particle complexes is mostly possible due to the magnetic moment produced by the individual particle complexes. Hence, it can be assumed that there is no interaction due to the hydrodynamic force between particles. Dipole-dipole interaction force is considered in this study by assuming two identical spherical particles as point dipoles. It has been reported that in a magnetophoretic bio-separation chip, magnetic particles tend to form chains [26], sheets [27], and membranes [28] because of interaction force between them. Different dipole models can be analyzed to obtain the exact dipole moment of the particles.

Particle-particle interaction in magnetophoretic bio-separation chip must be performed accurately because of its broad application in fluid transport in the presence of magnetic field, magnetic drug targeting [29] and biomedical sensing [30]. Due to the interaction force between particles, the trapping length of a bonded particle complex is smaller compared to the single particle. In a microfluidic channel, the interaction force can be of a particular of interest at the bottom of the channel where induced magnetic dipole moment between particles is quite high. Some studies have been performed in the past to reduce the effect of particle-particle interaction at the bottom of the channel. A model has been developed for disaggregation of superparamagnetic micro-particle complex clusters at the bottom of the channel with the help of induced magnetic dipole–dipole repulsion by Gao and van Reenen [31].

Scope of work

After the review of the literature, there appears to be an impending need and opportunity to comprehend the problem of particle-particle interaction in magnetophoretic bio-separation chips. To investigate the above research topic, a conceptual and analytical research outline is performed in this study. The main objective of this study is to examine the effect of inter-particle interaction on particle trajectories and how this effect can be implemented in force balance equations in a magnetophoretic bio-separation chip. This objective is achieved by performing a dipole based interaction force model and incorporating it into the particle transport analysis. Chapter 2 of this thesis presents the theoretical background of dipole-dipole interaction and different forces acting on a magnetic particle complex in the presence of an applied magnate c field. In chapter 3, simulations of magnetic flux gradient in OpenFOAM are discussed and particle modelling using coupled ordinary differential equations is performed. The simulation results and analysis are presented in chapter 4. In chapter 5, a summary of the entire work and some recommendations for future work are provided.

CHAPTER II

THEORETICAL BACKGROUND

Introduction

This chapter focuses on the theoretical approach of a dipole based model for particle interaction in a magnetophoretic bio-separation chip. Path integral and vector differential method are described in this chapter. In later part of this chapter, a dipole-dipole interaction force is simplified and incorporated with the other forces to predict the behavior and trajectory of cell-bead particle complexes.

Different models for particle interaction

Particle interaction force is an important phenomenon in a magnetophoretic bio-separation chip. The interaction force can be calculated either using a dipole based model or solving Laplace's equation for magnetostatics with multiple boundary conditions and finding Maxwell stress tensor for each particles [32]. Here Laplace's equation can be found using Gauss magnetization law where magnetic flux can be written as gradient of scalar quantity. Solution for Laplace's equation is difficult and cumbersome due to the boundary conditions for coordinates systems. The accuracy of the interaction force largely depends on the model used, physical properties of the particle complexes, angle between particles, their relative motion and the inter distance between the complexes [33]. The dipolar model (DM) is widely used to calculate the force between paramagnetic particles under the influence of magnetic field [34]. An analytical expression for the force between two magnetic particles can be derived if the particles are assumed as point dipoles.

Forces between magnetic dipoles

An analytical expression for interaction forces between two magnetic point dipoles is possible by using a closed form condition. As the magnetic dipole moment is a function of gradient of magnetic field, it is difficult to have a sense about the direction of the force. If the dipole moment is either parallel or perpendicular to the connector vector distance, then the force approximation will be much easier [35-39]. Two different approaches can be employed to develop an analytical expression for forces between magnetic dipoles [40]. These two methods are path integral approach and vector differentiation approach. In both cases, the connector vector length is large enough compared to the size of the dipoles.

A path integral approach

A geometric representation of two magnetic dipoles is shown in Fig. 5 where x and y are two magnetic elements. A magnetic force applied by an element x with current I_x on element b with current I_y is given by [40]

$$\vec{F}_{xy} = \frac{\mu_0}{4\pi} I_x I_y \oint\oint \frac{\vec{p}_y \times (\vec{p}_x \times \vec{R})}{R^3} d\theta_x d\theta_y \qquad (2.1)$$

where $\mu_0 = 4\pi \times 10^{-7}\, NA^{-2}$ is the magnetic constant, $\vec{p}_x$ and $\vec{p}_y$ are the vectors of path increment along circuit x and y, $\vec{R}$ is the vector distance from circuit path element $\vec{p}_x$ to $\vec{p}_y$.

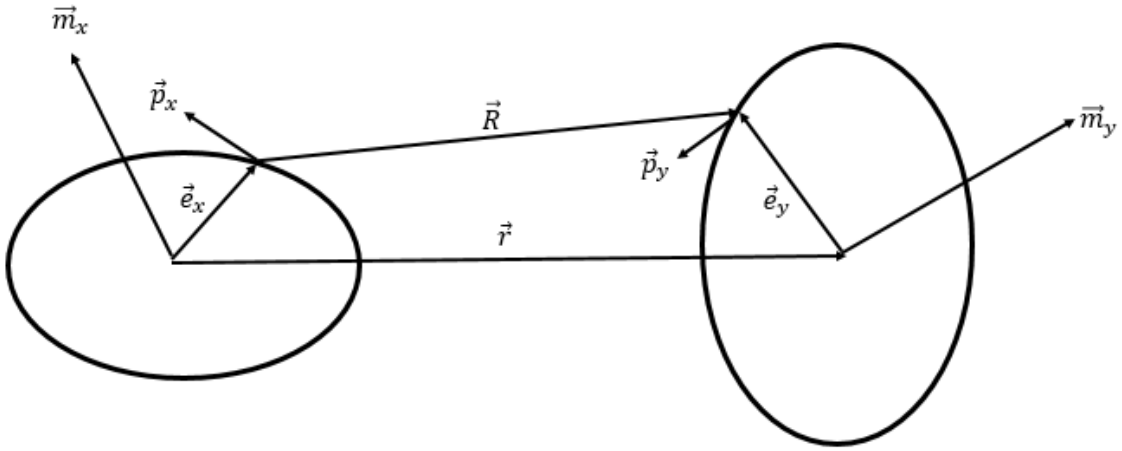

Figure 5: Geometric representation of two magnetic dipoles [40]

The magnetic dipole moments of these two dipoles can be defined as

$$\vec{m}_i = \frac{I_i}{2}\oint(\vec{e}_i \times \vec{p}_i)\, d\theta_i \ \text{, i = x or y} \tag{2.2}$$

From Fig 6, if the magnetic dipoles are plane circular circuits, the magnetic dipole moment can be written as

$$\vec{m} = m\hat{m} = \frac{I}{2}\oint(\vec{e} \times \vec{p})d\theta = \oint \vec{e} \times (ed\theta)\hat{p}$$

$$= (\hat{e} \times \hat{p})\left(\frac{Ie^2}{2}\int_0^{2\pi} d\theta\right) = (\pi e^2 I)(\hat{e} \times \hat{p}) \tag{2.3}$$

Where $\hat{m}$ is the unit dipole moment vector, θ is the angle from an axis to the magnetic moment.

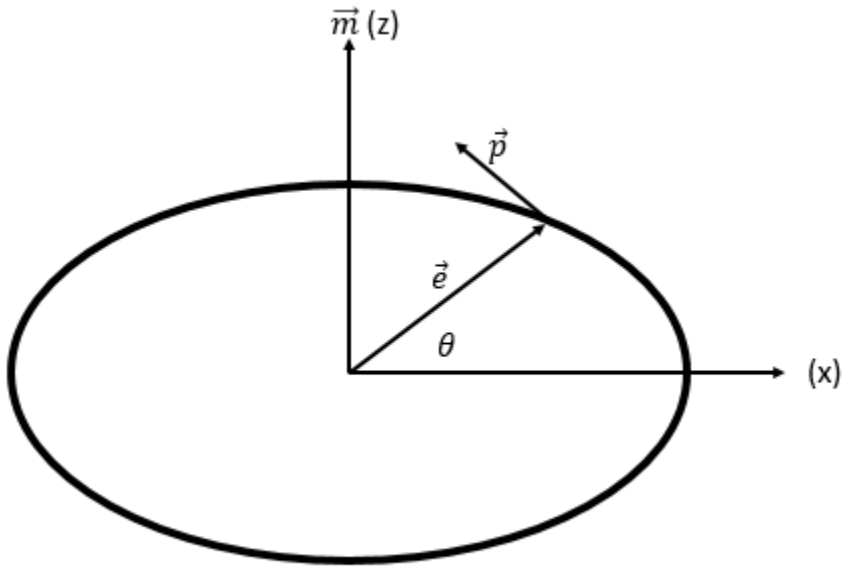

Figure 6: Geometric representation of magnetic dipole moment (generic) [40]

Expressing three unit vectors in terms of θ in a coordinate system:

$$\hat{m} = \begin{bmatrix} 0 \\ 0 \\ 1 \end{bmatrix} = \frac{\vec{m}}{m} \tag{2.4}$$

$$\hat{e} = \begin{bmatrix} cos\theta \\ sin\theta \\ 0 \end{bmatrix} = \frac{\vec{e}}{e} \tag{2.5}$$

$$\hat{p} = \begin{bmatrix} -sin\theta \\ cos\theta \\ 0 \end{bmatrix} = \frac{\vec{p}}{ed\theta} \tag{2.6}$$

$$\hat{e}.\hat{p} = \hat{e}.\hat{m} = \hat{p}.\hat{m} = 0 \tag{2.7}$$

$$\int \hat{e}\, d\theta = \int \hat{p} d\theta = \begin{bmatrix} 0 \\ 0 \\ 0 \end{bmatrix} = \vec{0} \tag{2.8}$$

Considering a coordinate system vector $\vec{w}$ in a circular dipole, we can write equation (2.4-2.6) as follows:

$$\vec{w} = \begin{bmatrix} x \\ y \\ z \end{bmatrix} \tag{2.9}$$

$$\int \vec{w}.\hat{m}\, d\theta = 2\pi\vec{w}.\hat{m} \tag{2.10}$$

$$\int \vec{w}.\hat{e}\, d\theta = \int (xcos\theta + ysin\theta)\, d\theta = 0 \tag{2.11}$$

$$\int \vec{w}.\hat{p}\, d\theta = \int (-xsin\theta + ycos\theta)\, d\theta = 0 \tag{2.12}$$

$$\int \hat{p}(\vec{w}.\hat{e})\, d\theta = \pi \begin{bmatrix} -y \\ x \\ 0 \end{bmatrix} = \pi\hat{m} \times \hat{w} \tag{2.13}$$

$$\int \hat{p}(\vec{w}.\hat{p})\, d\theta = \pi \begin{bmatrix} x \\ y \\ 0 \end{bmatrix} = \pi(\hat{w} - \hat{m}(\hat{m}.\hat{w})) \tag{2.14}$$

$$\int \hat{e}(\vec{w}.\hat{e})\, d\theta = \pi\big(\hat{w} - \hat{m}(\hat{m}.\hat{w})\big) \tag{2.15}$$

$$\int \hat{e}(\vec{w}.\hat{p})\, d\theta = -\pi\hat{m} \times \hat{w} \tag{2.16}$$

Considering two coordinate vectors $\vec{k}$ and $\vec{l}$ of circular magnetic dipoles, we can write following equations from Equations (2.4-2.6):

$$\vec{k} = \begin{bmatrix} x_k \\ y_k \\ z_k \end{bmatrix} \tag{2.17}$$

$$\vec{l} = \begin{bmatrix} x_l \\ y_l \\ z_l \end{bmatrix} \tag{2.18}$$

$$\int \big(\vec{k}.\hat{e}\big)\big(\vec{l}.\hat{p}\big)d\theta = \int (x_k cos\theta + y_k sin\theta)(-x_l sin\theta + y_l cos\theta)d\theta = \pi(x_k\, y_l - y_k x_l) = \pi(\vec{k} \times \vec{l})\hat{m} \tag{2.19}$$

$$\int(\vec{k}.\hat{e})(\vec{l}.\hat{e})d\theta = \pi\left(\vec{k}.\vec{l} - (\hat{k}.\hat{m})(\vec{l}.\hat{m})\right) = \pi(\hat{k}\times\hat{m}).(\vec{l}\times\hat{m}) \quad (2.20)$$

$$\int(\vec{k}.\hat{p})(\vec{l}.\hat{p})d\theta = \pi\left(\vec{k}.\vec{l} - (\hat{k}.\hat{m})(\vec{l}.\hat{m})\right) = \pi(\hat{k}\times\hat{m}).(\vec{l}\times\hat{m}) \quad (2.21)$$

$$\int(\vec{k}.\hat{e})(\vec{l}\times\hat{p})d\theta = \pi(\hat{k}\times\hat{m})\times\vec{l} \quad (2.22)$$

$$\int(\vec{k}.\hat{p})(\vec{l}\times\hat{e})d\theta = -\pi(\hat{k}\times\hat{m})\times\vec{l} \quad (2.23)$$

It can be assumed that separation vector $\vec{R}$ between the dipoles is larger than the size of the dipoles for far field approximation. Using Taylor series and disregarding higher order terms of 1/r, $\vec{R}$ value can be approximated as:

$$\vec{R} = \vec{r} + \Delta\vec{r} = \vec{r} + (\vec{e}_y - \vec{e}_x) \quad (2.24)$$

$$R^2 = r^2 + 2\vec{r}.\Delta\vec{r} + \Delta\vec{r}.\Delta\vec{r} = r^2\left(1 + 2\frac{\hat{r}.\Delta\vec{r}}{r} + \frac{\Delta\vec{r}.\Delta\vec{r}}{r^2}\right) \quad (2.25)$$

$$\frac{1}{R^3} \approx \frac{1}{r^3}\left(1 - 3\frac{\hat{r}.\Delta\vec{r}}{r} - \frac{3}{2}\frac{\Delta\vec{r}.\Delta\vec{r}}{r^2} + \frac{15}{2}\frac{(\hat{r}.\Delta\vec{r})^2}{r^2}\right) \quad (2.26)$$

Where $\vec{r}$ is the connector vector distance between the center of magnetic dipole x to y, $\Delta\vec{r}$ is the difference from center to current circuits which can be described as

$$\Delta\vec{r} = \vec{e}_y - \vec{e}_x$$

Substituting the equation (2.26) into equation (2.1) we can write:

$$\frac{\vec{p}_y\times(\vec{p}_x\times\vec{R})}{R^3} \approx \frac{\vec{p}_y\times(\vec{p}_x\times\vec{R})}{r^3}\left(1 - 3\frac{\hat{r}.\Delta\vec{r}}{r} - \frac{3}{2}\frac{\Delta\vec{r}.\Delta\vec{r}}{r^2} + \frac{15}{2}\frac{(\hat{r}.\Delta\vec{r})^2}{r^2}\right) \quad (2.27)$$

The integral value of the first term would be zero so it can be ignored. Then substituting equations (2.7) and (2.24) into equation (2.27).

$$\frac{\vec{p}_y\times(\vec{p}_x\times\vec{R})}{r^3}\left(-3\frac{\hat{r}.\Delta\vec{r}}{r}-\frac{3}{2}\frac{\Delta\vec{r}.\Delta\vec{r}}{r^2}+\frac{15}{2}\frac{(\hat{r}.\Delta\vec{r})^2}{r^2}\right)=\frac{\vec{p}_y\times\left(\vec{p}_x\times(\vec{r}+(\vec{e}_y-\vec{e}_x)\right)}{r^4}\left(-3\hat{r}.\Delta\vec{r}-\frac{3}{2}\frac{\Delta\vec{r}.\Delta\vec{r}}{r}+\frac{15}{2}\frac{(\hat{r}.\Delta\vec{r})^2}{r}\right)=\frac{1}{r^4}\left(\vec{p}_x(\vec{p}_y.\vec{r})-\vec{r}(\vec{p}_x.\vec{p}_y)-\vec{e}_y(\vec{p}_x.\vec{p}_y)-\vec{p}_x(\vec{p}_y.\vec{e}_x)+\vec{e}_x(\vec{p}_y.\vec{p}_x)\right)\times\left(-3\hat{r}.(\vec{e}_y-\vec{e}_x)-\frac{3}{2}\frac{(\vec{e}_y-\vec{e}_x)^2}{r}+\frac{15}{2}\frac{(\hat{r}.\vec{e}_y-\hat{r}.\vec{e}_x)^2}{r}\right) \quad (2.28)$$

In the above equation some terms have zero integral, rearranging the equation we can write

$$\frac{\vec{p}_y\times(\vec{p}_x\times\vec{R})}{r^3}\left(-3\frac{\hat{r}.\Delta\vec{r}}{r}-\frac{3}{2}\frac{\Delta\vec{r}.\Delta\vec{r}}{r^2}+\frac{15}{2}\frac{(\hat{r}.\Delta\vec{r})^2}{r^2}\right)=\frac{1}{r^4}\left(\vec{p}_x(\vec{p}_y.\vec{r})-\hat{r}(\vec{p}_x.\vec{p}_y)(3\left(\vec{e}_x.\vec{e}_y\right)(\vec{p}_x.\vec{p}_y)-15(\hat{r}.\vec{e}_x)(\hat{r}.\vec{e}_y)))+3\vec{e}_y(\vec{p}_x.\vec{p}_y)(\hat{r}.\vec{e}_y)+3(-\vec{p}_x(\vec{p}_y.\vec{e}_x)+\vec{e}_x(\vec{p}_y.\vec{p}_x)\right)(\hat{r}.\vec{e}_x) \quad (2.29)$$

By evaluating the above integrals using equations (2.10-2.16) and (2.18-2.23), it can be written as:

$$\oint\oint\vec{p}_x(\vec{p}_y.\hat{r})(\vec{e}_y.\vec{e}_x)d\theta_x d\theta_y=e_x{}^2e_y{}^2\int(\hat{p}_y.\hat{r})\int\hat{p}_x(\hat{e}_x.\hat{e}_y)d\theta_x d\theta_y==\frac{m_xm_y}{I_xI_y}\left(-(\hat{r}.\hat{m}_x)\hat{m}_y+(\hat{m}_x.\hat{m}_y)\hat{r}\right) \quad (2.30)$$

$$-\oint\oint\hat{r}(\vec{p}_x.\vec{p}_y)(\vec{e}_y.\vec{e}_x)d\theta_x d\theta_y=-\hat{r}e_x{}^2e_y{}^2\int\int(\vec{p}_x.\vec{p}_y)(\vec{e}_x.\vec{e}_y)\,d\theta_x d\theta_y=-\frac{2m_xm_y}{I_xI_y}\,(\hat{m}_x.\hat{m}_y)\hat{r} \quad (2.31)$$

$$-5\oint\oint\vec{p}_x(\vec{p}_y.\hat{r})(\hat{r}.\vec{e}_x)(\hat{r}.\vec{e}_y)d\theta_x d\theta_y=-5e_x{}^2e_y{}^2\int(\vec{p}_y.\hat{r})(\hat{r}.\vec{e}_y)\int\vec{p}_x(\hat{r}.\vec{e}_x)\,d\theta_x d\theta_y=0 \quad (2.32)$$

$$5\oint\oint\hat{r}(\vec{p}_x.\vec{p}_y)(\hat{r}.\vec{e}_x)(\hat{r}.\vec{e}_y)d\theta_x d\theta_y=5e_x{}^2e_y{}^2\int(\hat{r}.\vec{e}_y)\times\int(\vec{p}_x.\vec{p}_y)(\hat{r}.\vec{e}_x)\,d\theta_x d\theta_y=5\frac{m_xm_y}{I_xI_y}\,\hat{r}\left(\hat{m}_x.\hat{m}_y-(\vec{r}.\hat{m}_x)(\vec{r}.\hat{m}_y)\right) \quad (2.33)$$

$$-\oint\oint\vec{e}_y(\vec{p}_y.\vec{p}_x)(\hat{r}.\vec{e}_x)d\theta_x d\theta_y=-e_x{}^2e_y{}^2\int\hat{e}_y\int(\vec{p}_y.\vec{p}_x)(\hat{r}.\vec{e}_x)\,d\theta_x d\theta_y=\frac{m_xm_y}{I_xI_y}\left((\hat{m}_y.\hat{r})\hat{m}_x-(\hat{m}_y.\hat{m}_x)\hat{r}\right) \quad (2.34)$$

$$\oint\oint\vec{p}_x(\vec{p}_y.\vec{e}_x)(\hat{r}.\vec{e}_y)d\theta_x d\theta_y=-e_x{}^2e_y{}^2\int(\hat{r}.\vec{e}_y)\int\vec{p}_x(\vec{p}_y.\vec{e}_x)\,d\theta_x d\theta_y==\frac{m_xm_y}{I_xI_y}\,\left((\hat{r}.\hat{m}_x)\hat{m}_y-(\hat{m}_x.\hat{m}_y)\hat{r}\right) \quad (2.35)$$

$$-\oint\oint \vec{e}_x(\vec{p}_y.\vec{p}_x)(\hat{r}.\vec{e}_y)d\theta_x d\theta_y = -{e_x}^2{e_y}^2\int(\hat{r}.\hat{e}_y)\int \vec{e}_x(\vec{p}_y.\vec{p}_x)\,d\theta_x d\theta_y == \frac{m_x m_y}{l_x l_y}\left((\hat{r}.\hat{m}_x)\hat{m}_y - (\hat{m}_x.\hat{m}_y)\hat{r}\right) \quad (2.36)$$

From equations (2.28-2.36), we can get the interaction force of dipole x on dipole y as:

$$\vec{F}_{xy} = \frac{3\mu_0}{4\pi r^5}[(\vec{m}_x.\vec{r})\vec{m}_y + (\vec{m}_y.\vec{r})\vec{m}_x + (\vec{m}_x.\vec{m}_y)\vec{r} - \frac{5(\vec{m}_x.\vec{r})(\vec{m}_y.\vec{r})}{r^2}\vec{r}\,] \quad (2.37)$$

If dipole 1 has interaction on dipole 2, the above equation can be written as:

$$\vec{F} = \frac{3\mu_0}{4\pi r^5}[(\vec{m}_1.\vec{r})\vec{m}_2 + (\vec{m}_2.\vec{r})\vec{m}_1 + (\vec{m}_1.\vec{m}_2)\vec{r} - \frac{5(\vec{m}_1.\vec{r})(\vec{m}_2.\vec{r})}{r^2}\vec{r}\,] \quad (2.38)$$

Vector differential approach

Interaction force between dipoles can be derived using vector differential approach instead of the path integral approach. Magnetic field generated by dipole x to dipole y can be written as:

$$\vec{B}_{xy} = -\frac{\mu_0}{4\pi}\nabla\frac{\vec{m}_x.\vec{r}}{r^3} \quad (2.39)$$

Using potential energy consideration, force exerted by dipole x on dipole y can be expressed as:

$$\vec{F}_{xy} = -\nabla(-\vec{B}_{xy}.\vec{m}_y) = \nabla(\vec{B}_{xy}.\vec{m}_y) = -\frac{\mu_0}{4\pi}\nabla\left(\left(\nabla\frac{\vec{m}_x.\vec{r}}{r^3}\right).\vec{m}_y\right) \quad (2.40)$$

Where, $\nabla\frac{1}{r^n} = \begin{bmatrix}\partial/\partial x\\ \partial/\partial y\\ \partial/\partial z\end{bmatrix}\frac{1}{r^n} = -\frac{n}{r^{n+1}}\begin{bmatrix}x/r\\ y/r\\ z/r\end{bmatrix} = -\frac{n\vec{r}}{r^{n+2}}$ (2.41)

$$\nabla(\vec{w}_1.\vec{r}) = \begin{bmatrix}\partial/\partial x\\ \partial/\partial y\\ \partial/\partial z\end{bmatrix}(\vec{w}_1.\vec{r}) = \begin{bmatrix}\partial/\partial x(x_1x + y_1y + z_1z)\\ \partial/\partial y(x_1x + y_1y + z_1z)\\ \partial/\partial z(x_1x + y_1y + z_1z)\end{bmatrix} = \begin{matrix}x_1\\ y_1\\ z_1\end{matrix} = \vec{w}_1 \quad (2.42)$$

Using equations (2.41) and (2.42), equation (2.40) can be simplified as:

$$\vec{F}_{xy} = -\frac{\mu_0}{4\pi}\nabla\left(\left(\nabla\frac{\vec{m}_x.\vec{r}}{r^3}\right).\vec{m}_y\right)$$

$$= -\frac{\mu_0}{4\pi}\nabla\left(\left(\frac{1}{r^3}\nabla(\vec{m}_x.\vec{r}) + (\vec{m}_x.\vec{r})\nabla\frac{1}{r^3}\right).\vec{m}_y\right)$$

$$= -\frac{\mu_0}{4\pi}\nabla\left(\left(\frac{\vec{m}_x}{r^3} - (\vec{m}_x.\vec{r})\frac{3\vec{r}}{r^5}\right).\vec{m}_y\right)$$

$$= -\frac{\mu_0}{4\pi}\nabla\left(\frac{\vec{m}_x.\vec{m}_y}{r^3} - 3\frac{(\vec{m}_x.\vec{r})(\vec{m}_y.\vec{r})}{r^5}\right)$$

$$= -\frac{\mu_0}{4\pi}\left((\vec{m}_x.\vec{m}_y)\nabla\frac{1}{r^3} - 3(\vec{m}_x.\vec{r})(\vec{m}_y.\vec{r})\nabla\frac{1}{r^5} - 3\frac{(\vec{m}_y.\vec{r})}{r^5}\nabla(\vec{m}_x.\vec{r}) - 3\frac{(\vec{m}_x.\vec{r})}{r^5}\nabla(\vec{m}_y.\vec{r})\right)$$

$$\vec{F} = \frac{3\mu_0}{4\pi r^5}[(\vec{m}_x.\vec{r})\vec{m}_y + (\vec{m}_y.\vec{r})\vec{m}_x + (\vec{m}_x.\vec{m}_y)\vec{r} - \frac{5(\vec{m}_x.\vec{r})(\vec{m}_y.\vec{r})}{r^2}\vec{r}] \quad (2.43)$$

Which can also be written as

$$\vec{F} = \frac{3\mu_0}{4\pi r^5}[(\vec{m}_1.\vec{r})\vec{m}_2 + (\vec{m}_2.\vec{r})\vec{m}_1 + (\vec{m}_1.\vec{m}_2)\vec{r} - \frac{5(\vec{m}_1.\vec{r})(\vec{m}_2.\vec{r})}{r^2}\vec{r}] \quad (2.44)$$

Transport analysis of particle in bio-separation chip

Transport analysis of a particle is an important phenomenon in microfluidic devices. A schematic illustration of different forces acting on two cell-bead particle complexes during transport analysis is shown in Figure 7. Due to the applied magnetic field, a particle experiences different forces during its motion in the channel. Among the various forces acting on the particle, magnetic force, gravitational force, hydrodynamic drag force, and inter-particle interaction force are the dominant forces. Brownian motion can be ignored as the particle size is greater than 40 nanometers in this analysis. Due to the size, shape and concentration of the particles in this analysis, Van der Waal's force can also be neglected [41].

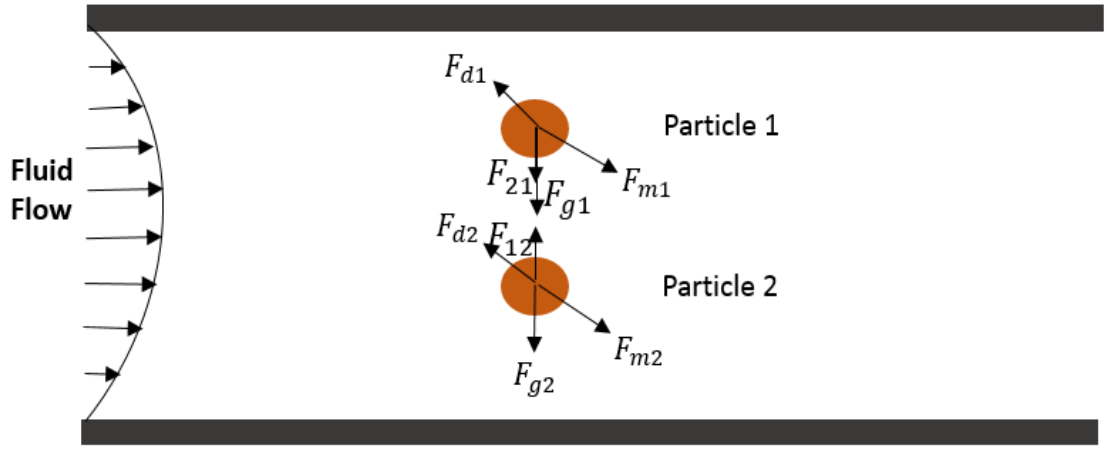

Figure 7: Schematic illustration of different forces acting on two cell-bead particle complexes subjected to an applied magnetic field. Hydrodynamic drag force, gravitational force, magnetic force, inter-particle interaction force are the dominant forces in the computational analysis. The applied magnetic field is parallel to the connector vector, $\vec{r}$.

Hydrodynamic drag force

A solid particle suspended in a fluid experiences hydrodynamic drag forces. If the Reynolds' number is low, which is the case with most microfluidic devices, the hydrodynamic drag force on a spherical particle can be approximated by Stokes' law:

$$\vec{F}_d = 6\pi R_p \eta(\vec{V}_f - \vec{V}_p) \tag{2.45}$$

Where R_p is the particle radius, η is the dynamic viscosity of the medium and $\vec{V}_f$ and $\vec{V}_p$ is the fluid and particle velocities, respectively.

If the flow is laminar throughout the channel, the fluid velocity can be written as:

$$\vec{V}_f = 6\frac{\mathrm{Q}}{\mathrm{hw\,h}}\frac{\mathrm{y}}{\mathrm{h}}\left(1 - \frac{\mathrm{y}}{\mathrm{h}}\right) \tag{2.46}$$

Where Q is the volumetric flow rate, h is the channel height, and w is the channel width.

Stokes drag force can be modified for non-spherical particles such as chain or fibers [42]. In such case, the drag force equation can be written as:

$$\vec{F}_d = 6\pi R_{pe}\eta(\vec{V}_f - \vec{V}_p)k \quad (2.47)$$

Where k is shape factor and R_{pe} is the equivalent radius of sphere having the same volume as the chain or fiber,

$$R_{pe} = \sqrt[3]{\frac{3v_{pe}}{4\pi}} \quad (2.48)$$

For cluster of n spheres

$$R_{pe} = n^{\frac{1}{3}}R_p \quad (2.49)$$

Drag force for liquid droplets can be given as:

$$\vec{F}_d = 6\pi R(\vec{V}_f - \vec{V}_p)\eta_f\left(\frac{1+\frac{2\eta_f}{3\eta_p}}{1+\frac{\eta_f}{\eta_p}}\right) \quad (2.50)$$

Where η_f and η_p is the dynamic viscosity of continuous fluid and discrete particles, respectively.

Magnetic force

The magnetic force acting on a particle is one of the dominant forces in a magnetophoretic bio-separation chip. In a magnetic bio-separation device, beads are attached to the target biomaterials. Due to the magnetic force exerted on the particle complex, the particle is pulled towards the bottom of the channel. Magnetic force on a particle complex is a function of magnetic moment of each magnetic particle around the cell and the magnetic field gradient in the channel.

$$\vec{F}_m = N(\vec{m}_b.\nabla)\vec{B} \quad (2.51)$$

Where $\vec{m}_b$ is the magnetic dipole moment of the particle, N is the number of beads, $\nabla\vec{B}$ is the magnetic flux gradient. It is assumed that magnetic force is proportional to the number of magnetic beads attached to each cell.

Magnetic moment of the beads can be written as:

$$\vec{m}_b = \rho_b V_b \vec{M}_b \quad (2.52)$$

Where ρ_b, V_b and $\vec{M}_b$ are the density, volume, and magnetization of the bead, respectively.

Gravitational force

At very low flow rates, the gravitational force can have an effect on trapping efficiency of a particle in a magnetic bio-separation chip. Thus, the gravitational force should be taken into account in the analysis of particle transport. The net gravitational force is due to the density difference of the particle and fluid inside the channel. As the density of the particle is higher than the density of the fluid, the particle would move toward the bottom of the chip. The net gravitational force can be written as

$$\vec{F}_g = (\rho_p - \rho_f)v_p\vec{g} \quad (2.53)$$

Where ρ_p and ρ_f are the densities of the particle and fluid, respectively, v_p is the volume of the particle, $\vec{g}$ is the gravitational acceleration.

Particle-particle interaction force

Particle interaction force is an important characteristic in a magnetophoretic bio-separation chip. A schematic illustration of magnetic dipole moments ($\boldsymbol{m_1}, \boldsymbol{m_2}$) of two cell-bead particle complexes under the influence of magnetic field in a magnetophoretic bio-separation chip is shown in Figure 8. It is assumed that magnetic dipole moment is in the direction of applied magnetic field, **B**. If the particles are assumed to be spherical point dipoles, the interaction force can be approximated by simplifying equation (2.38) depending on the direction of magnetic moment to the inter-particle distance. When the magnetic moment is parallel to the inter-particle distance, the equation (2.38) can be written as:

$$F = -\frac{3\mu_0}{2\pi r^4}(m_1 . m_2) \qquad (2.54)$$

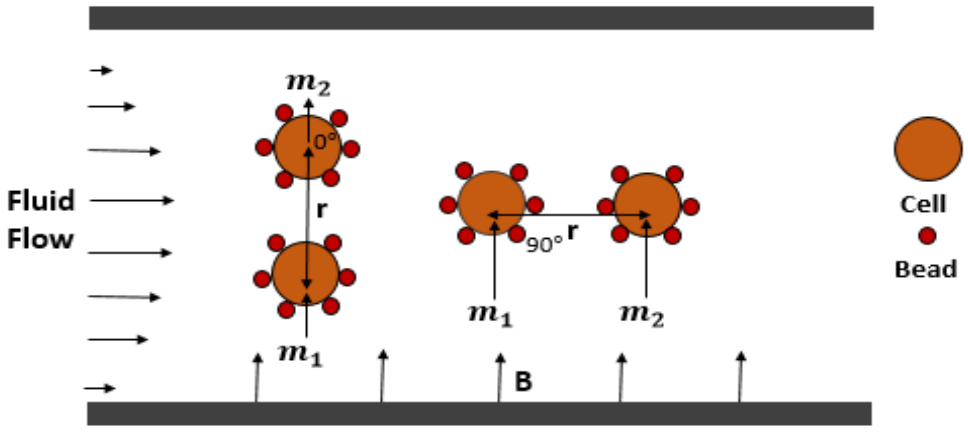

Figure 8: Schematic illustration of magnetic dipole moment ($\boldsymbol{m_1}, \boldsymbol{m_2}$) of two cell-bead particle complexes under the influence of magnetic field in a magnetophoretic bio-separation chip. It is assumed that the magnetic dipole moment is in the direction of applied magnetic field **B**.

When the magnetic moment is perpendicular to the inter-particle distance, the equation (2.38) can be written as:

$$F = \frac{3\mu_0}{4\pi r^4}(m_1 . m_2) \quad (2.55)$$

When the magnetic moment is at an angle of 45° to the inter-particle distance, the equation (2.38) can be written as:

$$F = -\frac{3\mu_0}{4\pi r^4}(0.086 m_1 . m_2) \quad (2.56)$$

Conclusion

In this chapter, the theoretical framework of a dipole based interaction force model in a magnetophoretic bio-separation chip is discussed. The interaction force between two magnetic particles was approximated by considering the particles as identical point dipoles. The transport analysis of a particle in a microfluidic chip is also discussed in this chapter. The next chapter will discuss the modelling and simulation of particle transport in a bio-separation chip.

CHAPTER III

MODELING AND SIMULATION

Introduction

This chapter describes the modeling and simulation of two cell-bead particle complexes in a magnetophoretic bio-separation chip. Magnetic flux gradients were simulated using OpenFOAM CFD software and were exported to MATLAB to obtain particle motion and trajectories in a microfluidic channel. The particle trajectories were obtained by solving a system of eight ordinary differential equations simultaneously using the fourth order Runge-Kutta method.

Magnetic flux gradients simulation

OpenFOAM CFD software was used to simulate magnetic flux gradients above an array of external magnets with opposing poles. The magnetic flux gradients at positions of 500-600 μm away from the surface of the magnets were used to obtain the gradients inside the microfluidic channel. The magnetic flux at different vertical position were then imported and stored in Matlab. Figures 9 and 10 show x- and y-components of magnetic field gradients at a vertical position of y=502 μm from the surface of the magnets. It has seen from these figures that the y-component of the magnetic field gradients in the channel is higher than the x-component. Similarly, x & y-components of magnetic field gradients at a vertical position of y=547 μm from the surface of the magnets are shown in Figures 11 and 12.

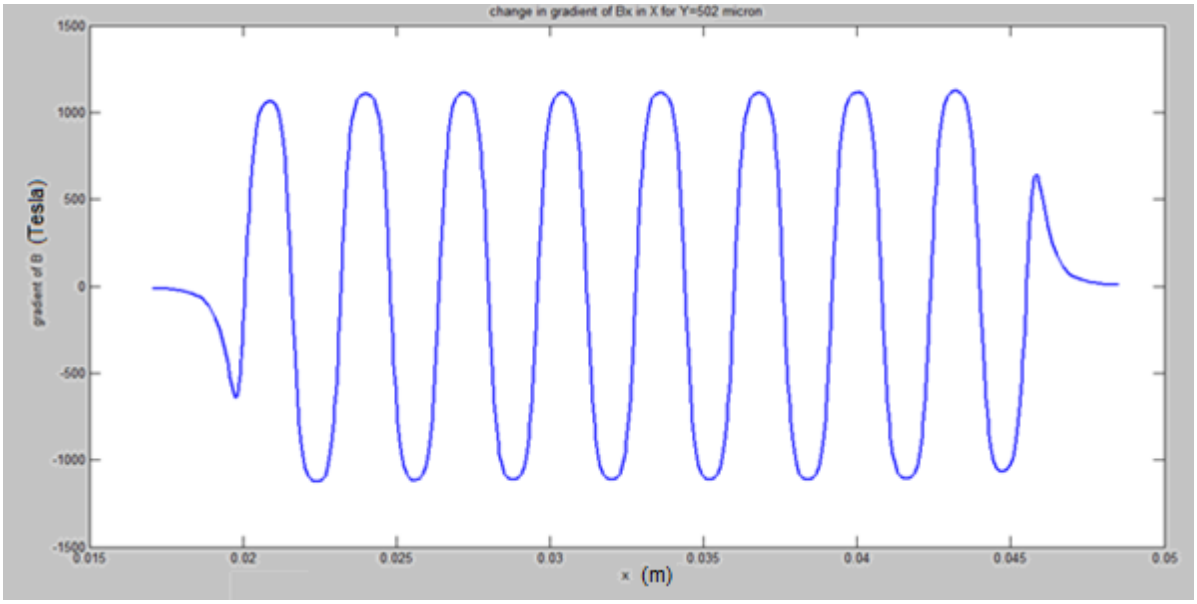

Figure 9: x-component of magnetic field gradient at a vertical position of y=502 μm from the surface of the magnets

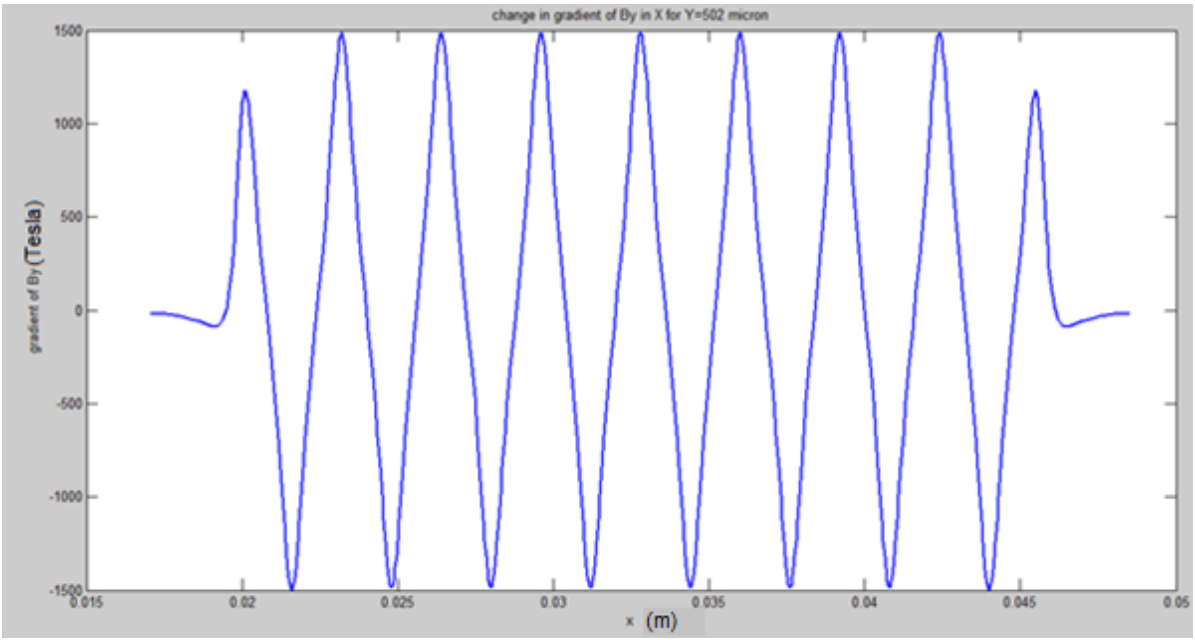

Figure 10: y-component of magnetic field gradient at a vertical position of y=502 μm from the surface of the magnets

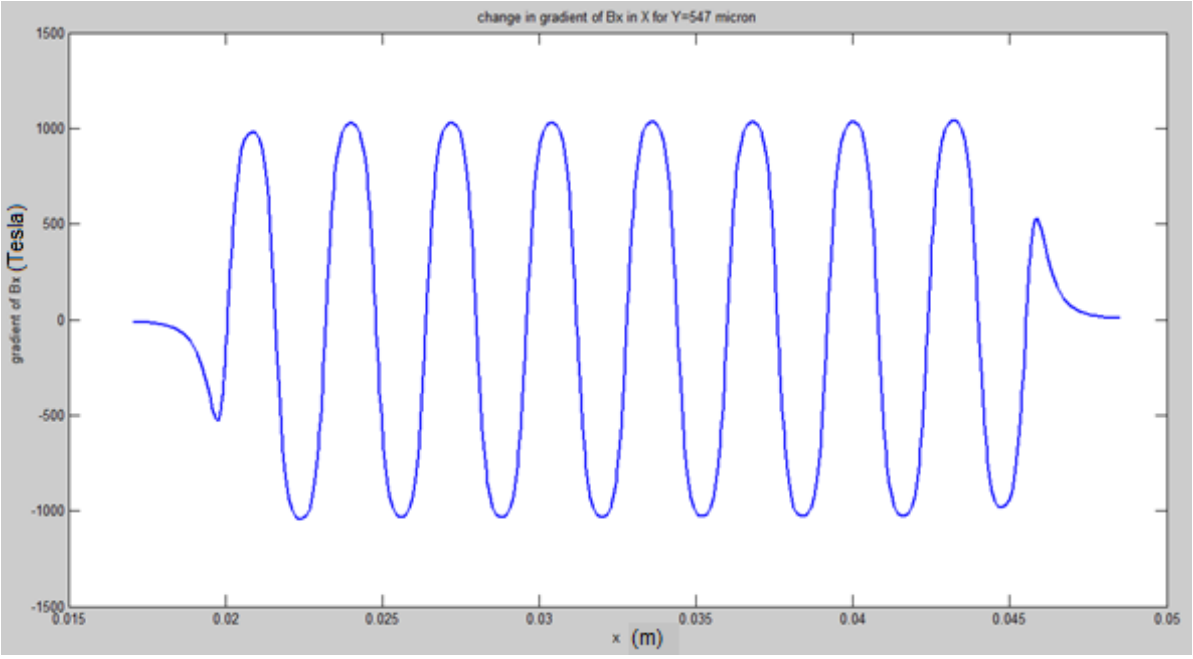

Figure 11: x-component of magnetic field gradient at a vertical position of y=547 µm from the surface of the magnets

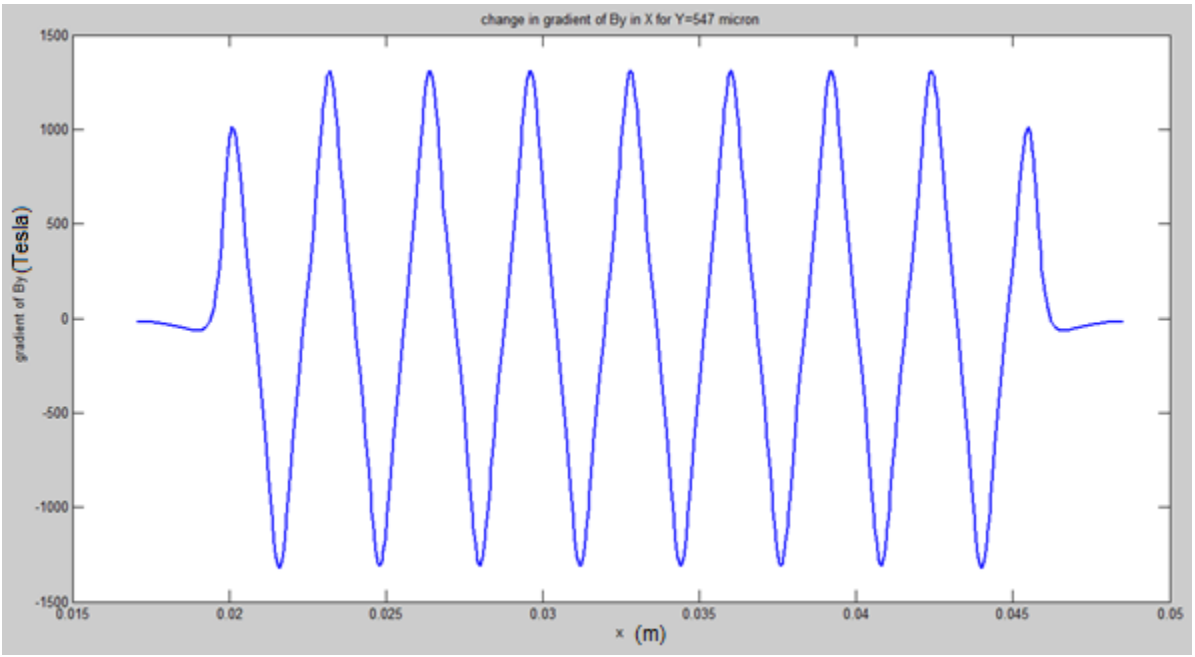

Figure 12: y- component of magnetic field gradient at a vertical position of y=547 µm from the surface of the magnets

Trajectory of Particle Complex

A 2-D particle motion under the influence of magnetic field is simulated using Matlab. The particle trajectory is predicted using different forces acting on the particle including the magnetic force, drag force, gravitational force, and particle-particle interaction force. Horizontal and vertical components of magnetic flux are considered in the simulation. When the magnetic moment is parallel to the connector vector, the motion of the particles in the channel can be predicted by applying Newton's second law in the x and y directions:

Force balance for particle 1 in the x-direction:

$$m_{p1}\frac{dv_{p1,x}}{dt} = F_{d1,x} + F_{m1,x} \tag{3.1}$$

Force balance for particle 1 in the y-direction:

$$m_{p1}\frac{dv_{p1,y}}{dt} = F_{d1,y} + F_{m1,y} + F_{g1} + F_{21} \tag{3.2}$$

Force balance for particle 2 in the x-direction:

$$m_{p2}\frac{dv_{p2,x}}{dt} = F_{d2,x} + F_{m2,x} \tag{3.3}$$

Force balance for particle 2 in the y-direction:

$$m_{p2}\frac{dv_{p2,y}}{dt} = F_{d2,y} + F_{m2,y} + F_{g2} + F_{12} \tag{3.4}$$

Substituting equations (2.45), (2.46), (2.47), (2.51), (2.53) and (2.54) in equations 3.1-3.4, and simplifying, we can write:

$$\frac{dv_{p1,y}}{dt} + kv_{p1,y} = n_y \tag{3.5}$$

$$\frac{dv_{p1,x}}{dt} + kv_{p1,x} = n_x \quad (3.6)$$

$$\frac{dv_{p2,y}}{dt} + kv_{p2,y} = n_{y'} \quad (3.7)$$

$$\frac{dv_{p2,x}}{dt} + kv_{p2,x} = n_{x'} \quad (3.8)$$

Where

$$k = \frac{6\pi R_{p1}\boldsymbol{\eta}}{m_{p1}} = \frac{6\pi R_{p2}\boldsymbol{\eta}}{m_{p2}}$$

$$n_y = \frac{N\rho_b V_b \vec{M}_b(\nabla.\vec{B}_y) + (\rho_p - \rho_f)v_{p1}\vec{g} + \frac{3\mu_0}{2m_{p1}\pi D^4 |r/D|^4}(-m_1 m_2)}{m_{p1}}$$

$$n_x = \frac{36\pi R_{p1}\eta Q}{m_{p1}hw}\frac{y}{h}(1-\frac{y}{h}) + \frac{N\rho_b V_b \vec{M}_b(\nabla.\vec{B}_x)}{m_{p1}}$$

$$n_{y'} = \frac{N\rho_b V_b \vec{M}_b(\nabla.\vec{B}_y) + (\rho_p - \rho_f)v_{p2}\vec{g} + \frac{3\mu_0}{2\pi D^4 |r/D|^4}(-m_1 m_2)}{m_{p2}}$$

$$n_{x'} = \frac{36\pi R_{p2}\eta Q}{m_{p2}hw}\frac{y}{h}(1-\frac{y}{h}) + \frac{N\rho_b V_b \vec{M}_b(\nabla.\vec{B}_x)}{m_{p2}}$$

Similarity, when the applied magnetic field is perpendicular to the connector vector, the equations of motion for particles 1 and 2 are as follows:

Force balance for particle 1 in the x-direction:

$$m_{p1}\frac{dv_{p1,x}}{dt} = F_{d1,x} + F_{m1,x} + F_{12} \quad (3.9)$$

Force balance for particle 1 in the y-direction:

$$m_{p1}\frac{dv_{p1,y}}{dt} = F_{d1,y} + F_{m1,y} + F_{g1} \tag{3.10}$$

Force balance for particle 2 in the x-direction:

$$m_{p2}\frac{dv_{p2,x}}{dt} = F_{d2,x} + F_{m2,x} + F_{12} \tag{3.11}$$

Force balance for particle 2 in the y-direction:

$$m_{p2}\frac{dv_{p2,y}}{dt} = F_{d2,y} + F_{m2,y} + F_{g2} \tag{3.12}$$

Again, by substituting equations (2.45), (2.46), (2.47), (2.51), (2.53) and (2.54) in equations 3.9-3.12, we can write:

$$\frac{\mathrm{dv_{p1,y}}}{\mathrm{dt}} + \mathrm{kv_{p1,y}} = \mathrm{p_y} \tag{3.13}$$

$$\frac{\mathrm{dv_{p1,x}}}{\mathrm{dt}} + \mathrm{kv_{p1,x}} = \mathrm{p_x} \tag{3.14}$$

$$\frac{\mathrm{dv_{p2,y}}}{\mathrm{dt}} + \mathrm{kv_{p2,y}} = \mathrm{p_{y'}} \tag{3.15}$$

$$\frac{\mathrm{dv_{p2,x}}}{\mathrm{dt}} + \mathrm{kv_{p2,x}} = \mathrm{p_{x'}} \tag{3.16}$$

Where

$$\mathrm{k} = \frac{6\pi \mathrm{R_{p1}}\eta}{\mathrm{m_{p1}}} = \frac{6\pi \mathrm{R_{p2}}\eta}{\mathrm{m_{p2}}}$$

$$\mathrm{p_y} = \frac{N\rho_b\, V_b\, \vec{M}_b(\nabla.\vec{B}_y) + (\rho_p - \rho_f)\mathrm{v_{p1}}\vec{\mathrm{g}}}{\mathrm{m_{p1}}}$$

$$p_x = \frac{36\pi R_{p1}\eta \mathrm{Q}}{m_{p1}hw}\frac{y}{h}\left(1 - \frac{y}{h}\right) + \frac{N\rho_b\, V_b\, \vec{M}_b(\nabla.\vec{B}_x)}{m_{p1}} + \frac{3\mu_0}{4m_{p1}\pi D^4\, |r/D|^4}(m_1 m_2)$$

$$p_{y'} = \frac{N\rho_b V_b \vec{M}_b(\nabla.\vec{B}_y) + (\rho_p - \rho_f)\mathrm{v_{p2}}\vec{\mathrm{g}}}{m_{p2}}$$

$$p_{x'} = \frac{36\pi R_{p2}\eta \mathrm{Q}}{m_{p2}hw}\frac{y}{h}\left(1 - \frac{y}{h}\right) + \frac{N\rho_b V_b \vec{M}_b(\nabla.\vec{B}_x)}{m_{p2}} + \frac{3\mu_0}{4m_{p2}\pi D^4 |r/D|^4}(m_1 m_2)$$

The particle trajectories within the microfluidic channel were simulated by solving equations (3.5-3.8) and equations (3.13-3.16). The numerical simulation was performed using the fourth order Runge-Kutta technique. MATLAB cannot solve second order ordinary differential equations. Thus, the above equations were first integrated and converted into 8 first order ordinary differential equations (ODEs) to obtain the positions of the particles. Equations (3.5-3.8) constitute a coupled system of ODEs. A similar approach was employed for equations (3.13-3.16).

When the applied magnetic field is perpendicular to the connector vector, the coupled system of equations can be written as:

$$\frac{dv_{p1,y}}{dt} = \mathrm{n_y} - \mathrm{kv_{p1,y}} \tag{3.17}$$

$$v_{p1,y} = \frac{dy_1}{dt} \tag{3.18}$$

$$\frac{dv_{p1,x}}{dt} = \mathrm{n_x} - \mathrm{kv_{p1,x}} \tag{3.19}$$

$$v_{p1,x} = \frac{dx_1}{dt} \tag{3.20}$$

$$\frac{dv_{p2,y}}{dt} = \mathrm{n_y} - \mathrm{kv_{p2,y}} \tag{3.21}$$

$$v_{p2,y} = \frac{dy_2}{dt} \tag{3.22}$$

$$\frac{dv_{p2,x}}{dt} = \mathrm{n_x} - \mathrm{kv_{p2,x}} \tag{3.23}$$

$$v_{p2,x} = \frac{dx_2}{dt} \tag{3.24}$$

The above equations were solved subject to initial conditions for position of $x_1(0)$, $y_1(0)$, $x_2(0)$, $y_2(0)$ and velocity of $v_{p1,x}(0)$, $v_{p1,y}(0)$, $v_{p2,x}(0)$, $v_{p2,y}(0)$ of the particles. Then, the change in the vertical and horizontal positions of the particles were calculated from the initial position where the particle started its transport in the channel to determine the travel paths of each particle. Similar approaches were employed for cases where the applied magnetic field were parallel or at an angle of 45° to the connector vector.

Conclusion

In this chapter, the simulation of magnetic field gradients and modelling of the particle transport in microfluidic channel were presented. The numerical simulation was performed using the fourth order Runge Kutta scheme by solving eight coupled ordinary differential equations. The following chapter will discuss the results of a parametric study to investigate the effects of various parameters on the particle motion.

CHAPTER IV

RESULTS AND DISCUSSION

Introduction

In this chapter, trajectories of two cell-bead particle complexes in a microfluidic channel are analyzed and presented. Additionally, a parametric study has been performed to investigate the effect of particle-particle interaction on particle motion and trajectories within a microfluidic channel.

Parametric study of two particle complexes in a microchannel

Trajectories of two cell-bead particle complexes were first investigated to predict the interaction force as they moved through a microchannel. The trajectories of the particles were simulated in Matlab by solving a system of coupled ordinary differential equations. The effects of sample flow rate, number of beads per cell, and cell size are studied. Simulations were performed for the following three cases:

1) Case I: The applied magnetic field is parallel (0°) to the connector vector.
2) Case II: The angle between the applied magnetic field and the connector vector is 45°.
3) Case III: The applied magnetic field is perpendicular (90°) to the connector vector.

Case I

At first, simulations were performed for a case where the magnetic field was parallel (same direction) to the connector vector. The direction of the magnetic moment of the particles was assumed to be in the direction of applied magnetic field. Then, the interaction force of the particle complexes was simplified and used in the ordinary differential equations. In this case,

a parametric study was performed by varying flow rate, number of beads per cell, and cell size. The comparison of trajectories of two particle complexes with a single particle was also performed. The connector vector distance was also varied to investigate its effect on the interaction force and particle trajectories.

Effect of flow rate on particle interaction

Varying the sample flow rate in a magnetophoretic bio-separation chip can affect the particle trapping length and trapping efficiency. In the first sets of simulations, the inter-particle distance or center to center distance of the particles were assumed to be the same as the particle diameter. When the particles travel along the channel, they are attracted to each other due to an attractive dipole-dipole interaction force. This attraction force is basically due to the assumption that the particles are point dipoles. Figure 13 depicts the trajectories of two cell-bead particle complexes at various flow rates. The number of beads per cell, cell size, and bead size were 10, 10 µm, 1 µm, respectively. The results indicate that the particle trapping length increases almost linearly as the flow rates increases. It is assumed that the first particle starts its journey from a vertical position of 100 μm and the second particle starts from a vertical position of 90 μm since the spacing between the particles complexes is assumed to be the same as the particle diameter (i.e. r=D). After travelling some distance, the particles are pulled together and form a single bonded particle due to an attractive magnetic force between them. The bonded particle then follows its own trajectory in the microfluidic channel. It is observed that particles are bonded after they travel approximately 30 μm from the top of the channel. It is also observed that as the flow rates increase, the time required for the particles to bond together increases as well.

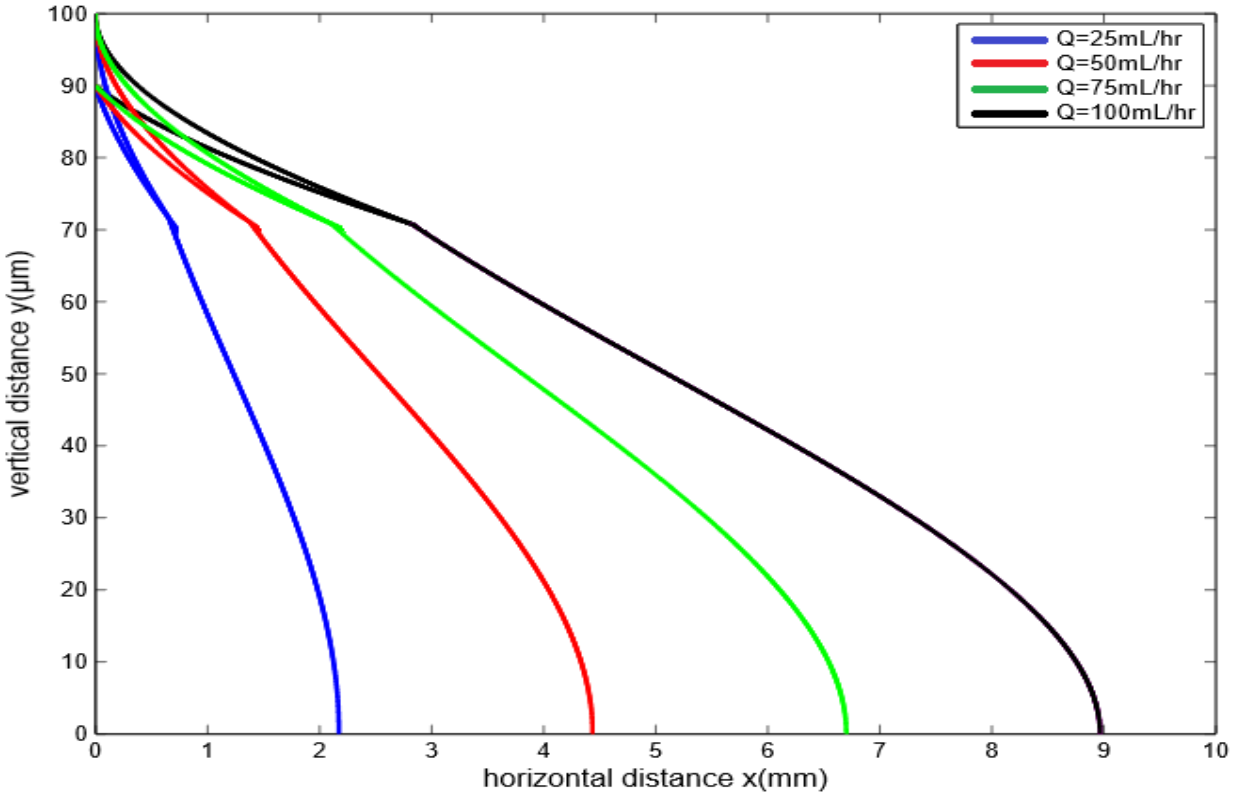

Figure 13: Trajectories of two cell-bead particle complexes for a case where the applied magnetic field is parallel to the connector vector at various flow rates. The distance between the particle complexes is the same as the particle diameter (r=D). The number of beads per cell, cell size, bead size is 10, 10 μm, 1 μm, respectively. After travelling some distance,the particles are attracted to each other and bonded together. The bonded particle follows its own trajectory in the microfluidic channel.

The bonded particle is not spherical. They form a chain like structure due to the presence of the external magnetic field. The modeling of the bonded particles is performed by introducing

a shape factor to calculate the drag force for a non-spherical particle. When the particles are bonded together, their magnetic moments increase by a factor of two but the drag force does not increase significantly. An equivalent particle radius was calculated assuming that the bonded particles were a cluster of spheres and was used to calculate the drag force. A shape factor value of k=1.12 was used in the simulation because the chain was aggregate of two spherical particles [42]. The other parameters of particle modelling in the microfluidic channel remained the same but the effective mass and volume were twice that of a single particle. It is observed that the bonded particle is trapped at the bottom of the channel earlier compared to the single particle. This is because a higher magnetic force is exerted on the bonded particle as compared to the hydrodynamic drag force.

Figure 14 shows similar simulation results as the previous case except that the particle-particle spacing is twice that of the particle diameter (i.e. r=2D). In this case, the first particle starts its journey from a vertical position of 100 μm while the second particle starts from a vertical position of 80μm. The results show that it takes more time for particles to be pulled together and bonded and travel approximately two-third of the channel height when they bond together. Similar to the r=D case, as the flow rates increases, it takes more time for particles to bond together. However, in this case, each bonded particle has a larger trapping length compared to the r=D case. This is because for the r=D case, the particles are bonded sooner, and the bonded particle experiences a larger magnetic force and is pulled down faster towards the bottom of the channel.

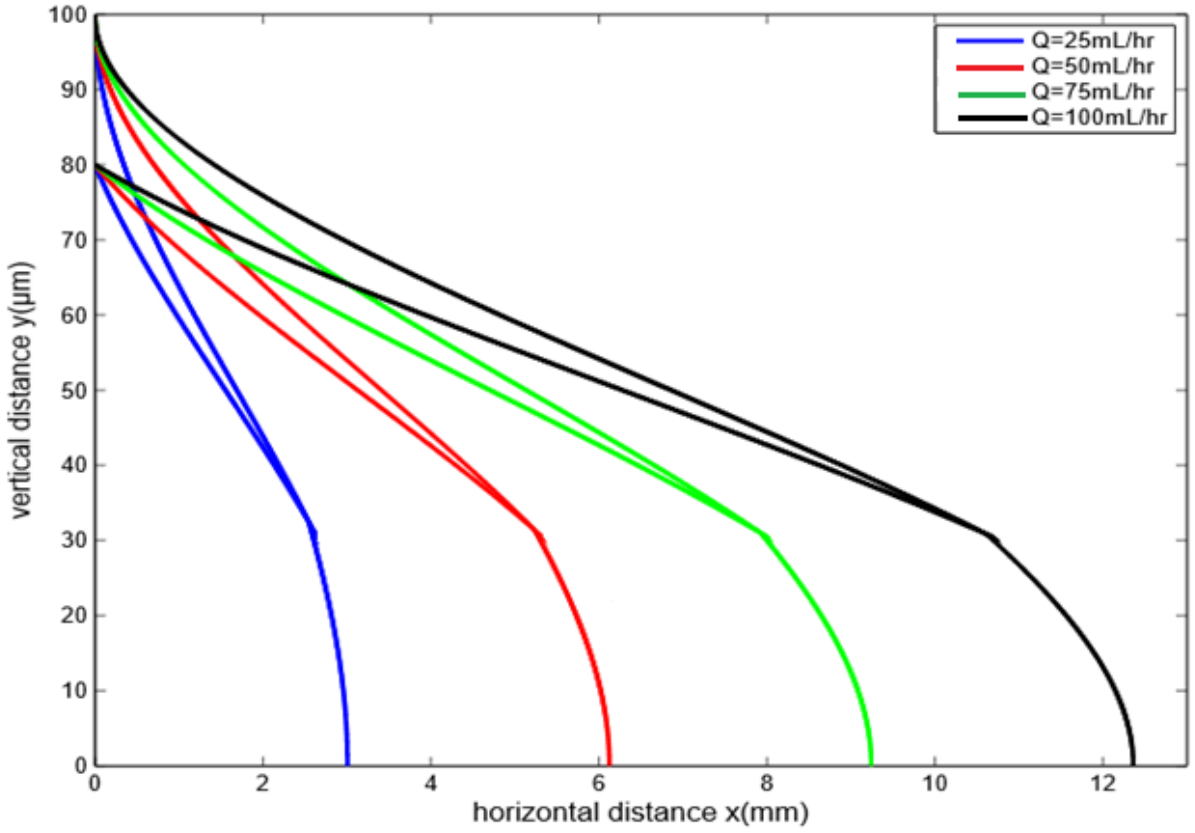

Figure 14: Trajectories of two cell-bead particle complexes for a case where the applied magnetic field is parallel to the connector vector at various flow rates. The distance between particle complexes is twice the particle diameter (r=2D). The number of beads per cell, cell size, bead size is 10, 10 μm, 1 μm, respectively.

Effect of number of beads per cell on particle interaction

The number of beads that are attached to each cell can have a significant effect on particle-particle interaction in a bio-separation chip. Figure 15 shows the simulation results for an inter-particle spacing of r=D at various number of beads per cell. As the number of beads per cell increases, the magnetic moment around the particle complexes increase as well. Thus, the particle complexes with more number of beads are attracted to each other at a much faster rate and bonded together sooner. As a result, the trapping length decreases as the number of beads per cell increases.

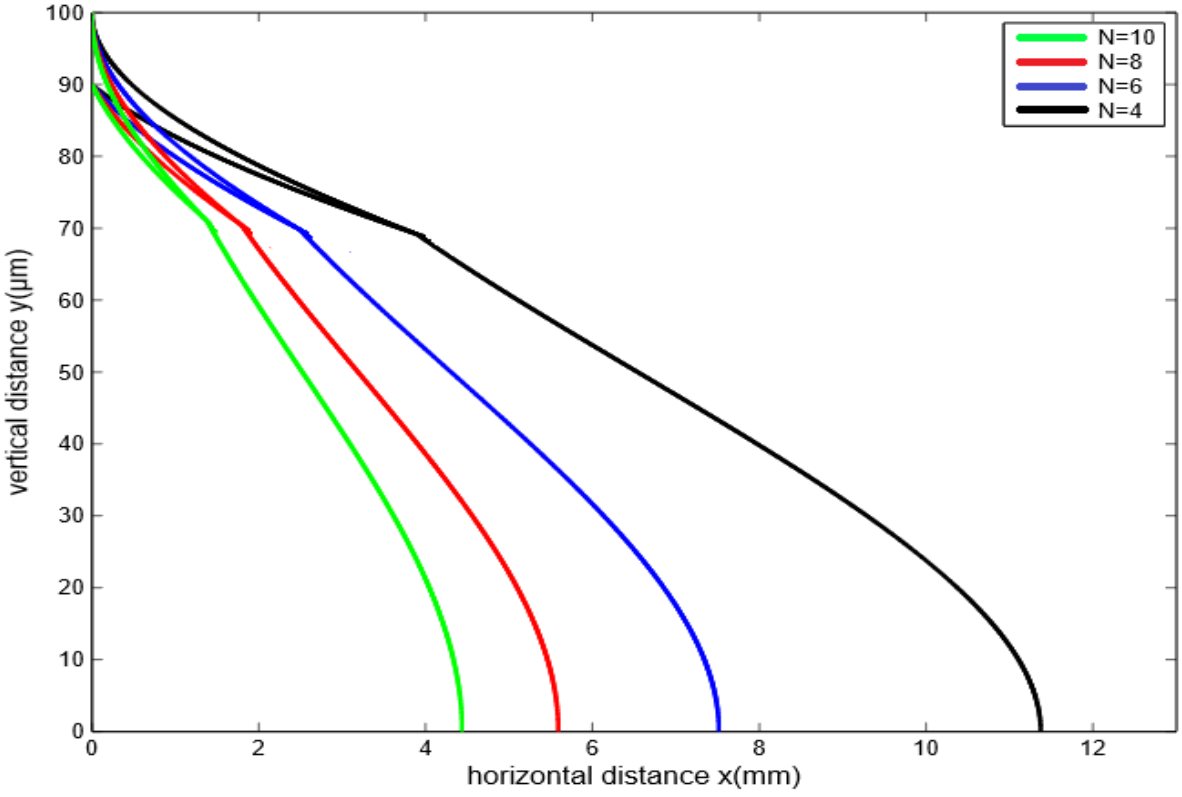

Figure 15: Trajectories of two cell-bead particle complexes for a case where the applied magnetic field is parallel to the connector vector at various number of beads/cell. The distance between particle complexes is the same as the particle diameter (r=D). The cell size, bead size,

flow rate is 10 µm, 1 µm, 50 mL/hr, respectively.

A similar approach has been employed in figure 16 except the particle-particle spacing is twice the particle diameter (r=2D). In this case, the particle bonding takes place after they travel approximately 65μm from the top of the channel. It is also seen that the trapping length is larger compared to the r=D case.

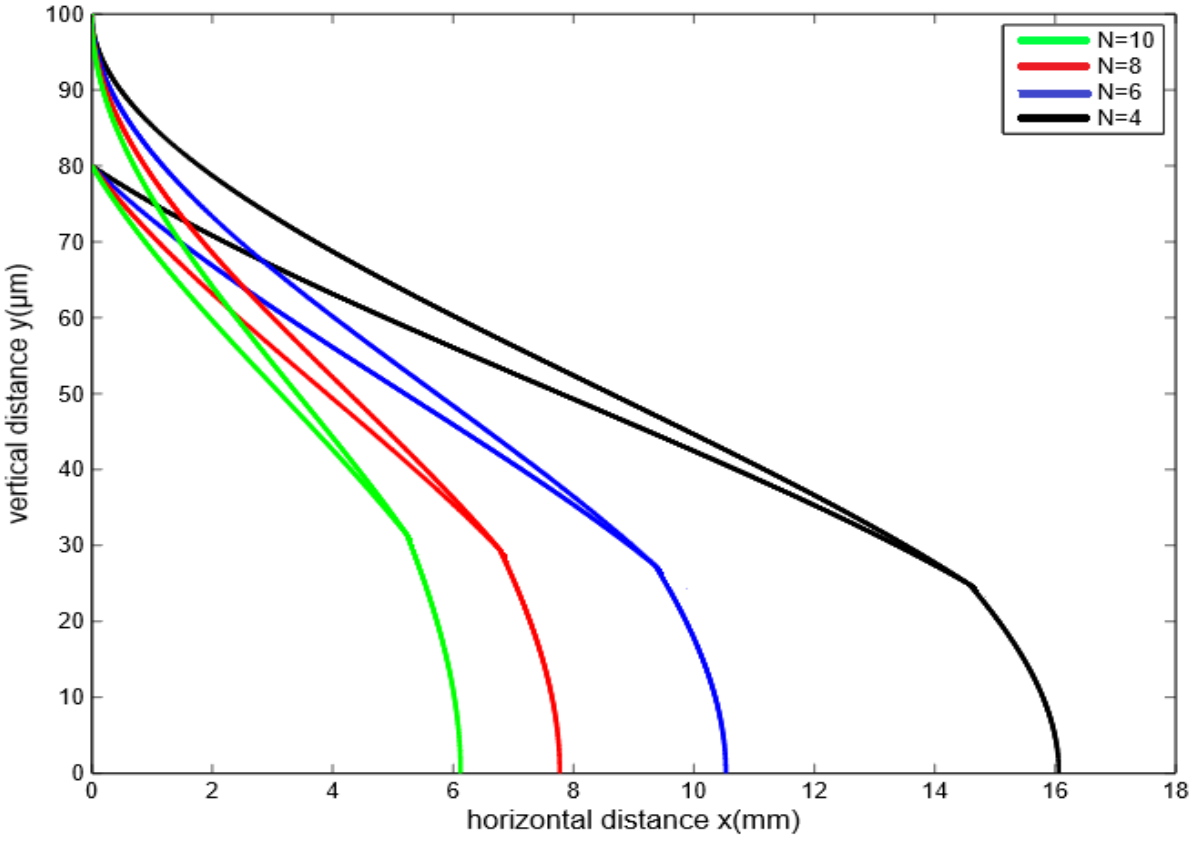

Figure 16: Trajectories of two cell-bead particle complexes for a case where the applied magnetic field is parallel to the connector vector at various number of beads/cell. The distance between particle complexes is twice the particle diameter (r=2D). The cell size, bead size, flow rate is 10 µm, 1 µm, 50 mL/hr, respectively.

Effect of cell size in particle interaction

For a given number of beads per cell, the interaction force between particle complexes is different depending on the cell size. Figure 17 shows the particle trajectories for three different cell sizes at an inter-particle distance of r=D. The particle bonding is found to occur after the complexes travel approximately $30\mu m$ from the top of the channel. The results also show that it takes more time for the particles to be trapped on the bottom of the channel as the cell size increase. Thus, it can be said that the particle interaction is less dominant for larger cell sizes if the number of beads per cell is kept the same. In figure 18, the simulation results are similar to Figure 17 except the inter-particle spacing is twice the particle diameter. Similar behavior can be observed from this figure except that the trapping length is larger than that of r=D.

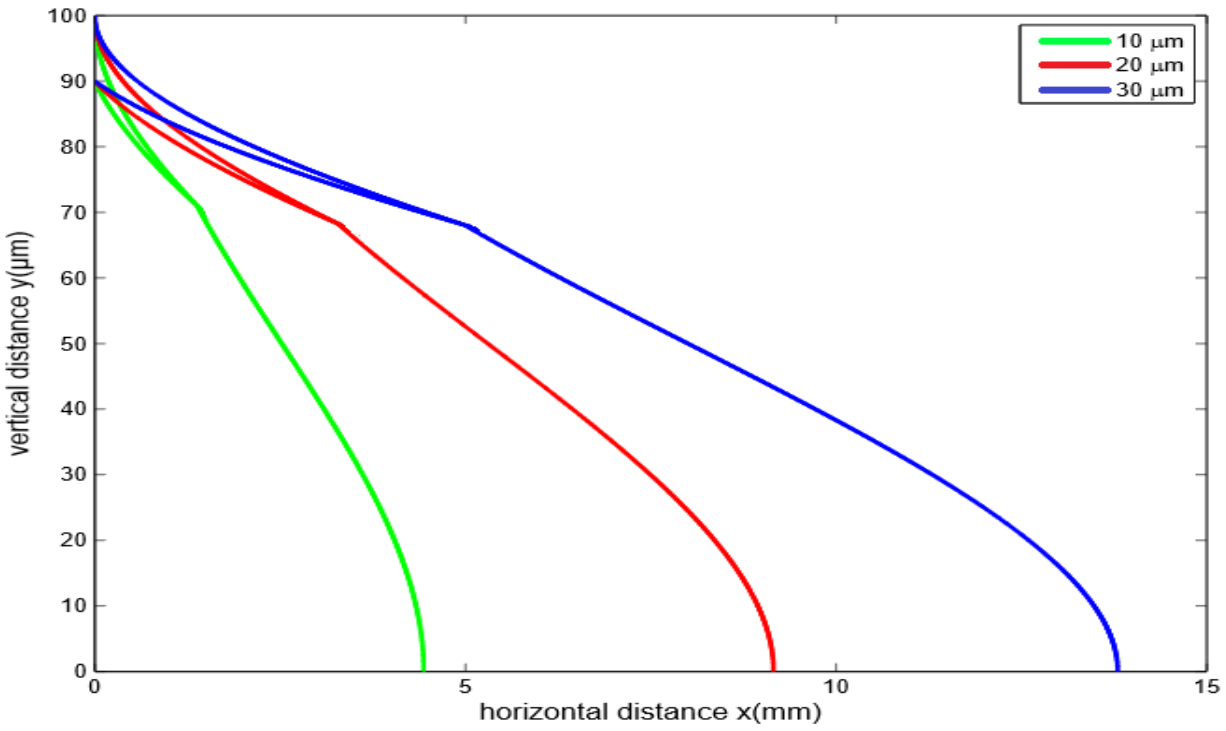

Figure 17: Trajectories of two cell-bead particle complexes for a case where the applied magnetic field is parallel to the connector vector at various cell sizes. The distance between particle complexes is the same as the particle diameter (r=D). The flow rate, number of beads, bead size is 50 mL/hr, 10,1 µm, respectively.

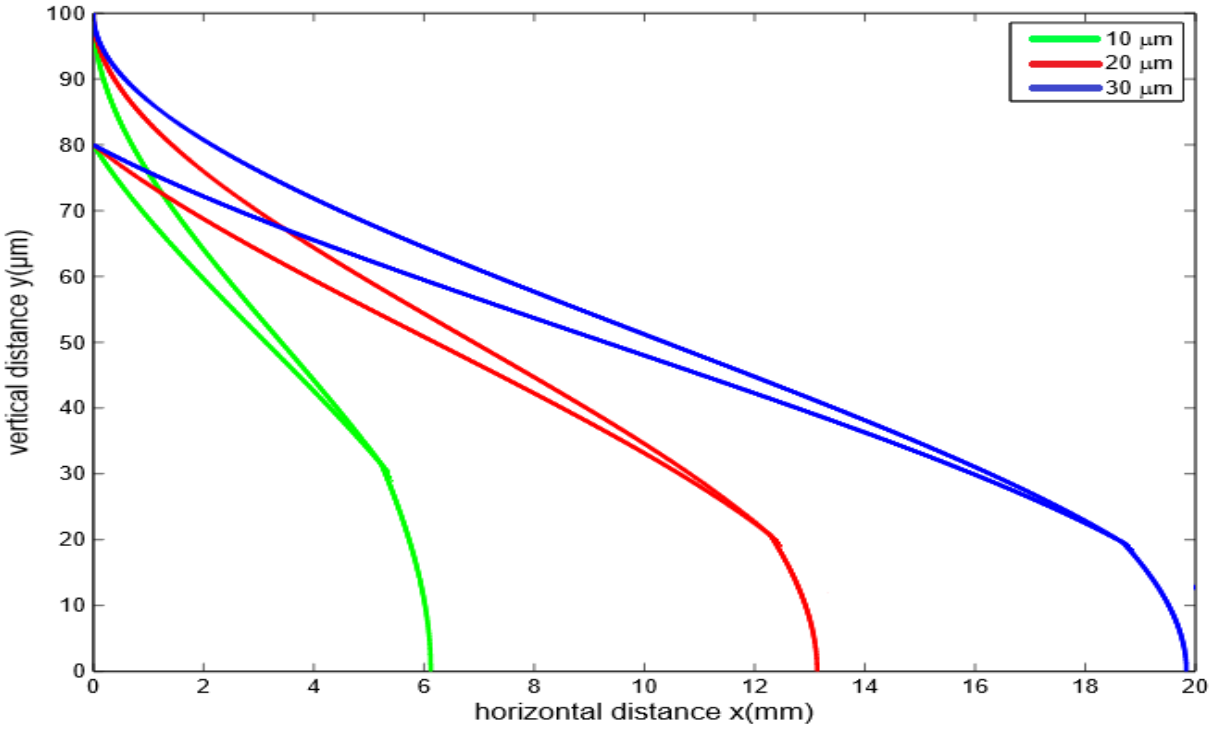

Figure 18: Trajectories of two cell-bead particle complexes for a case where the applied magnetic field is parallel to the connector vector at various cell sizes. The distance between particle complexes is twice the particle diameter (r=2D). The flow rate, bead size is 50 mL/hr 1 µm, respectively.

Case II

The simulation is performed for a case where applied magnetic field is at an angle of 45° to the inter-particle distance. It is assumed that magnetic moment of the particles complexes occurs at an angle of 45 degrees to the connector vector distance. In this case, the magnetic moment is reduced considerably compared to the previous case where the magnetic moment was parallel to the connector vector. For this reason, all particles trajectories were found to be similar to the parallel case except that the trapping length is longer. A similar parametric study was performed to investigate the effect flow rate, number of beads per cell and cells size on particle-particle interaction inside the channel.

Effect of flow rate on particle interaction

Figure 19 and 20 depict the effect of flow rate at inter-particle distances r=D and r=2D for a case where the applied magnetic field is at an angle of 45° to the inter-particle distance. The results show that it takes more time for the particles to be bonded and pulled towards the bottom of the channel compared to the zero degree case. It is seen that for an inter-particle distance of r=D, the particles complexes are bonded after travelling 33μm from the top of the channel while the particles are bonded after they travel a vertical distance of approximately 77 μm for r=2D. For all sample flow rates, the trapping lengths of the bonded particles are longer than case I since the interaction force is smaller than the zero degree case where the magnetic moment was parallel to the inter-particle distance.

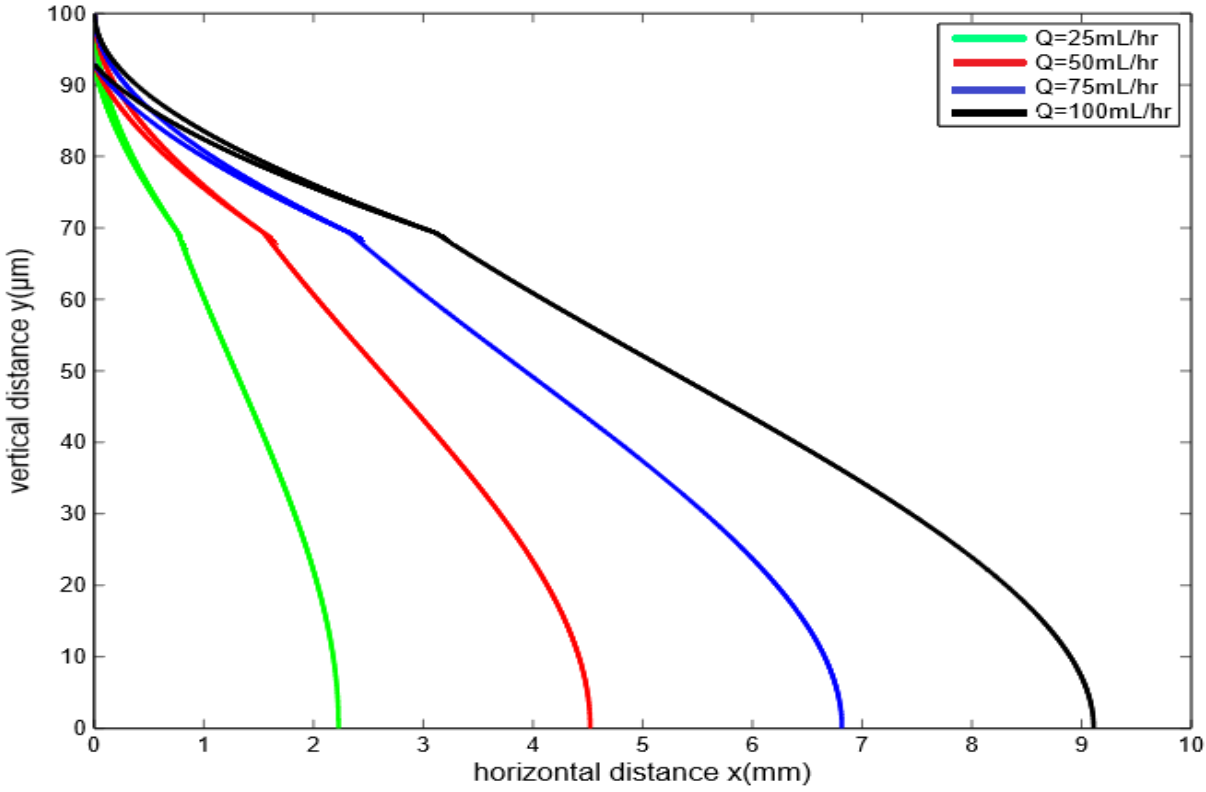

Figure 19: Trajectories of two cell-bead particle complexes for a case where the applied magnetic field is at an angle of 45 degrees to the connector vector at various flow rates. The distance between the particle complexes is the same as the particle diameter (r=D). The number of beads per cell, cell size, bead size is 10, 10 μm, 1 μm, respectively.

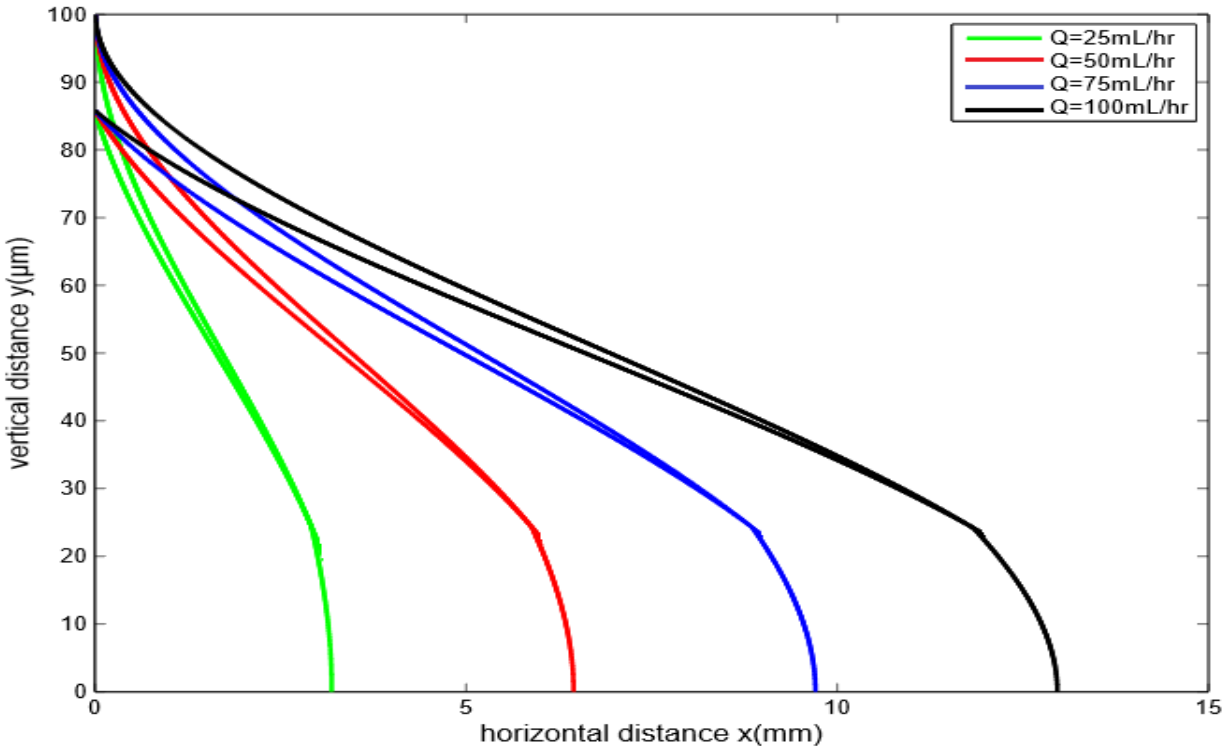

Figure 20: Trajectories of two cell-bead particle complexes for a case where the applied magnetic field is at an angle of 45 degrees to the connector vector at various flow rates. The distance between particle complexes is twice the particle diameter (r=2D). The number of beads per cell, cell size, bead size is 10, 10 μm, 1 μm, respectively.

Effect of number of beads per cell on particle interaction

Effects of number of beads per cell on particle trajectory and particle-particle interaction for a case where magnetic field is at an angle of 45 degrees to the inter-particle distance are shown in Fig. 21 and 22. For the r=D case, the first particle starts its journey from of position of (7.07 μm, 100 μm) while the second particle starts from (0 μm, 92.93 μm). For the r=2D case, the starting positions of the first and second particles are (14.14 μm, 100 μm) and (0 μm, 85.86 μm) in the channel. In both cases the trend is similar to the zero degree case except that the

trapping length is longer. The trapping lengths of the particles decrease with increasing the number of beads attached to the cell. However, for the 45 degrees case, particle bonding takes more time than the parallel case because the interaction force between the particles is smaller.

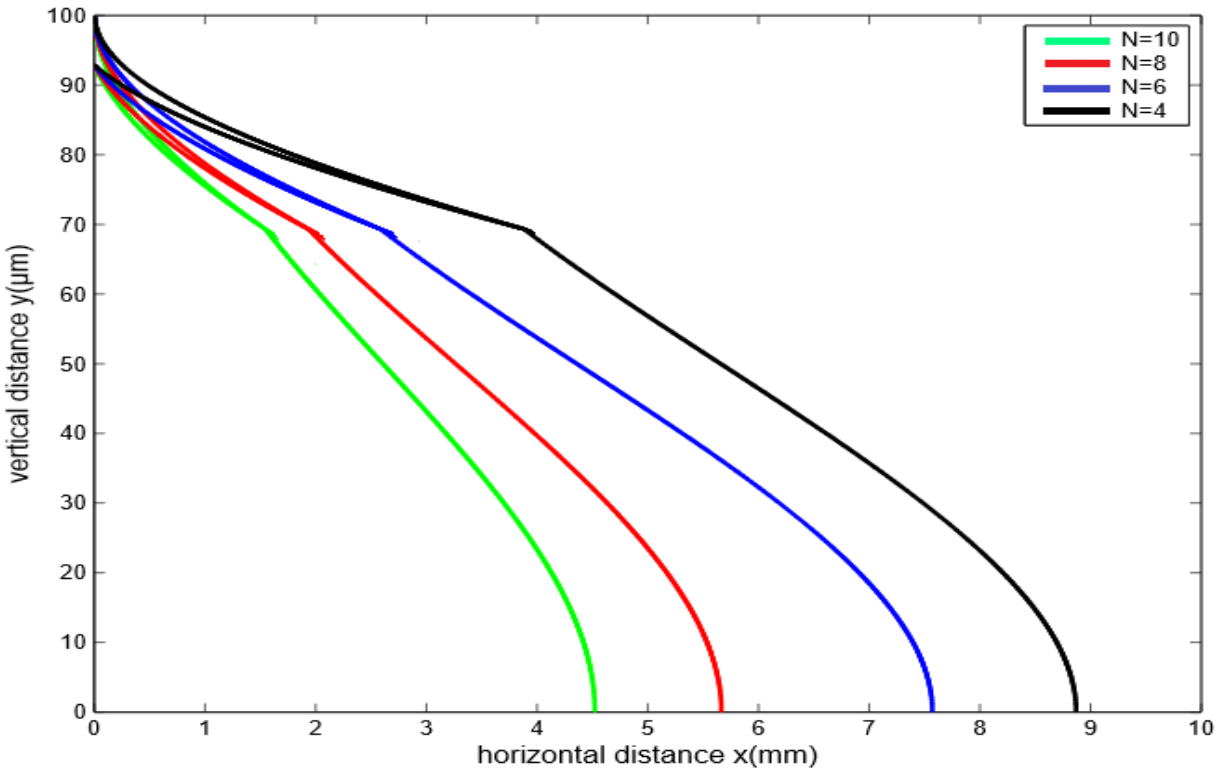

Figure 21: Trajectories of two cell-bead particle complexes for a case where the applied magnetic field is at an angle of 45 degrees to the connector vector at various number of beads/cell. The distance between particle complexes is the same as the particle diameter (r=D). The cell size, bead size, flow rate is 10 μm, 1 μm, 50 mL/hr, respectively.

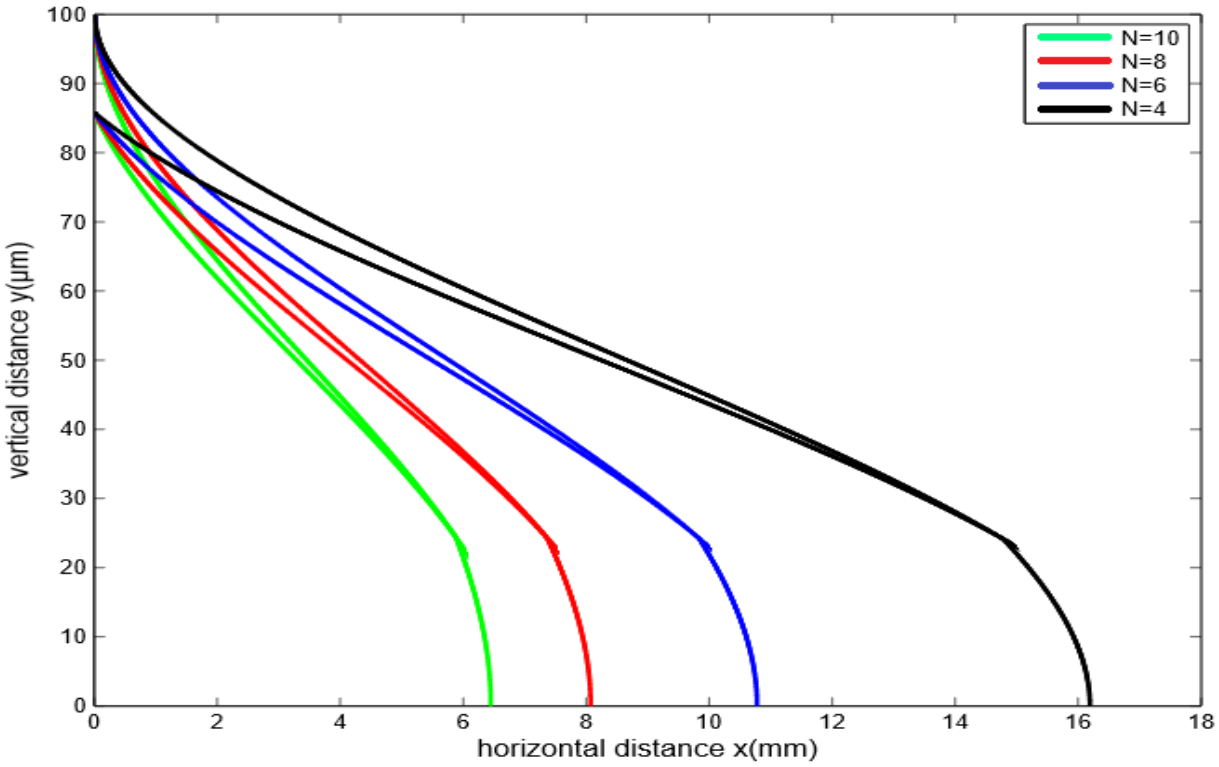

Figure 22: Trajectories of two cell-bead particle complexes for a case where the applied magnetic field is at an angle of 45 degrees to the connector vector at various number of beads /cell. The distance between particle complexes is twice the particle diameter (r=2D). The cell size, bead size, flow rate is 10 µm, 1 µm, 50 mL/hr, respectively.

Effect of cell size on particle interaction

Figures 23 and 24 show the effect of cell size on particle interaction and trajectories for two different cases of r=D and r =2D. In both cases, the trapping lengths are larger than the case where the applied magnetic field is parallel to the inter-particle connector vector. For the r=D case, the particles are bonded together after travelling a vertical distance of 33 μm from the top of the channel. Also, as expected the trapping length increases with increasing the cell size because the drag force is larger for larger cell sizes.

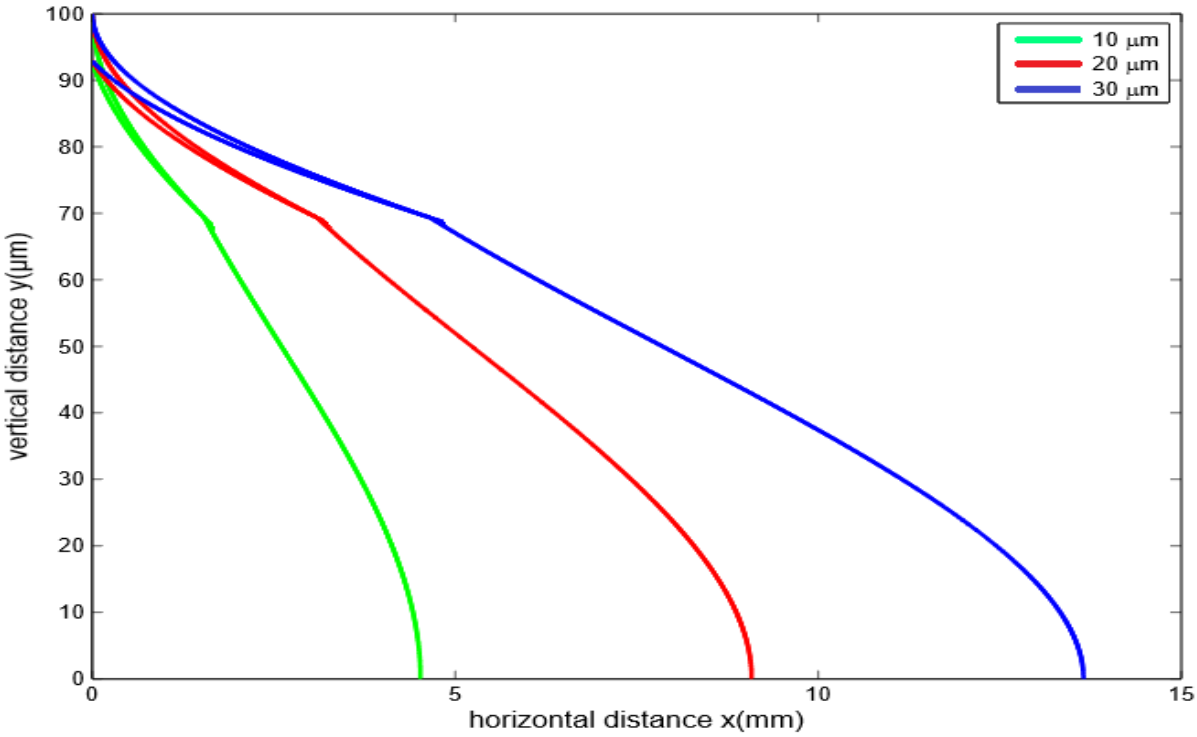

Figure 23: Trajectories of two cell-bead particle complexes for a case where the applied magnetic field is at an angle of 45 degrees to the connector vector at various cell sizes. The distance between particle complexes is the same as the particle diameter (r=D). The flow rate, number of bead, bead size is 50 mL/hr, 10, 1 µm, respectively.

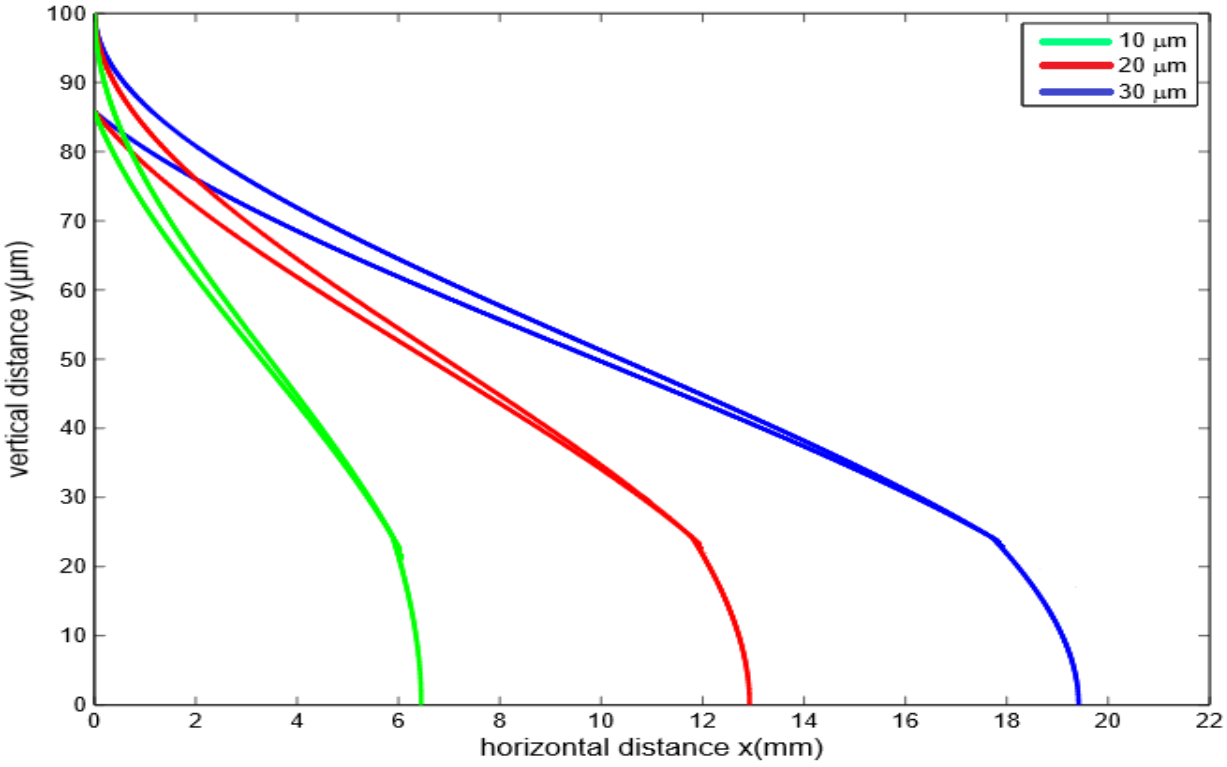

Figure 24: Trajectories of two cell-bead particle complexes for a case where the applied magnetic field is at an angle of 45 degrees to the connector vector at various cell sizes. The distance between particle complexes is twice the particle diameter (r=2D). The flow rate, number of bead, bead size is 50 mL/hr, 10, 1 µm, respectively.

Case III

Simulations were also performed for a case where the magnetic field is in perpendicular to the connector vector distance. Figure 25 shows the trajectories of two cell-bead particle complexes. The distance between 1st and 2nd particle complexes is twice that of the particle diameter (r=2D). The number of beads per cell, cell size, bead size, and flow rate are 10, 10 µm, 1 µm, 50 mL/hr, respectively. It is observed that the particles do not bond in this case and each particle follow its own trajectory. This is because as shown in Equation 2.55, when the

connector vector is aligned perpendicular to the dipoles, the interaction force between the particles is repulsive, and particle bonding does not occur.

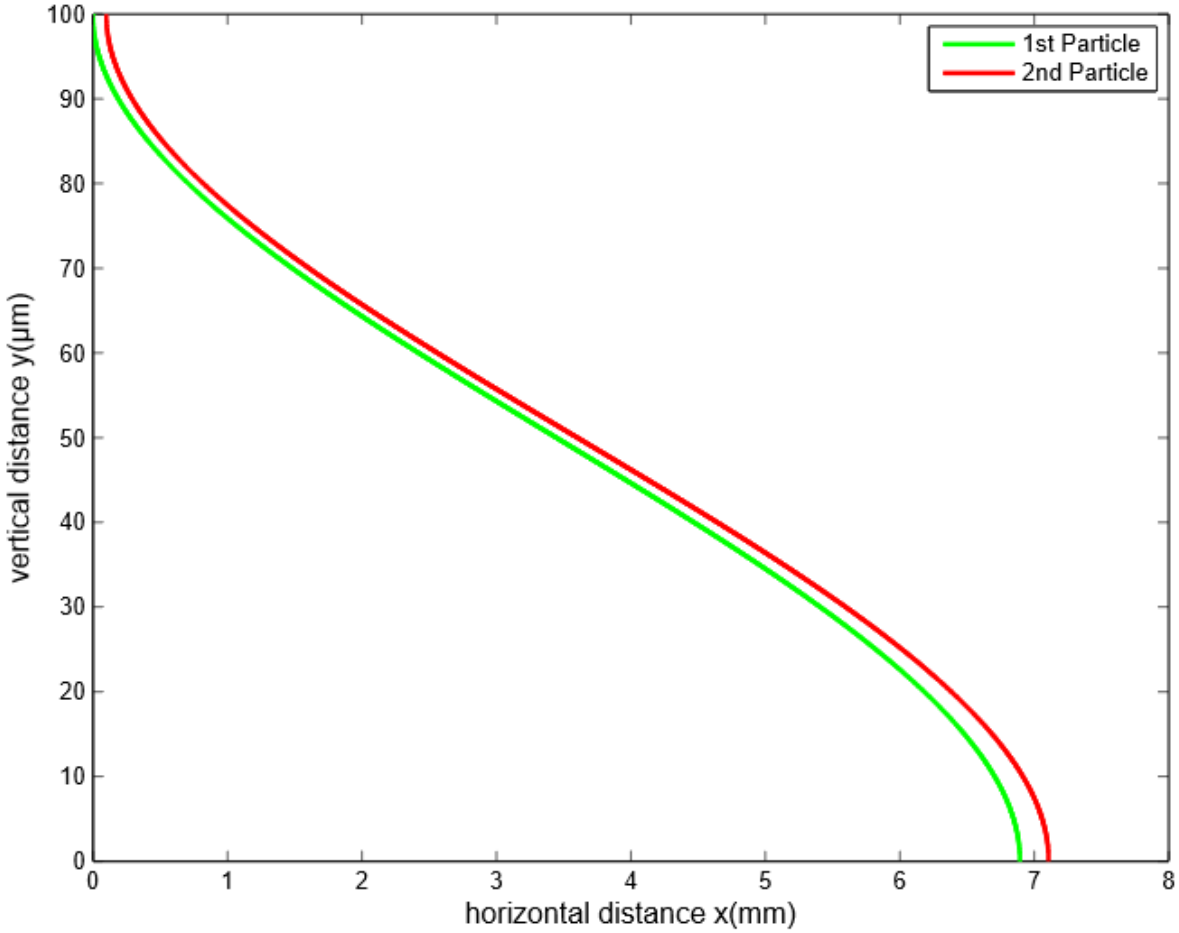

Figure 25: Trajectories of two cell-bead particle complexes for a case where the applied magnetic field is in perpendicular to the connector vector. The number of beads per cell, cell size, bead size, flow rate is 10, 10 µm, 1 µm, 50 mL/hr, respectively.

Comparison of trajectories of two particle complexes with single particle trajectory

Figure 26 depicts a comparison between the trajectories of the 0° and 45° cases with a single particle trajectory. In all cases, the cell size, bead size, number of bead, and flow rate is "10 µm, 1 µm, 10, 50 mL/hr" respectively. The results show that that the particle-particle interaction is more dominant for the 0° case than the 45° case. It is also observed that the trapping length for single particle is larger than both 0° and 45° cases.

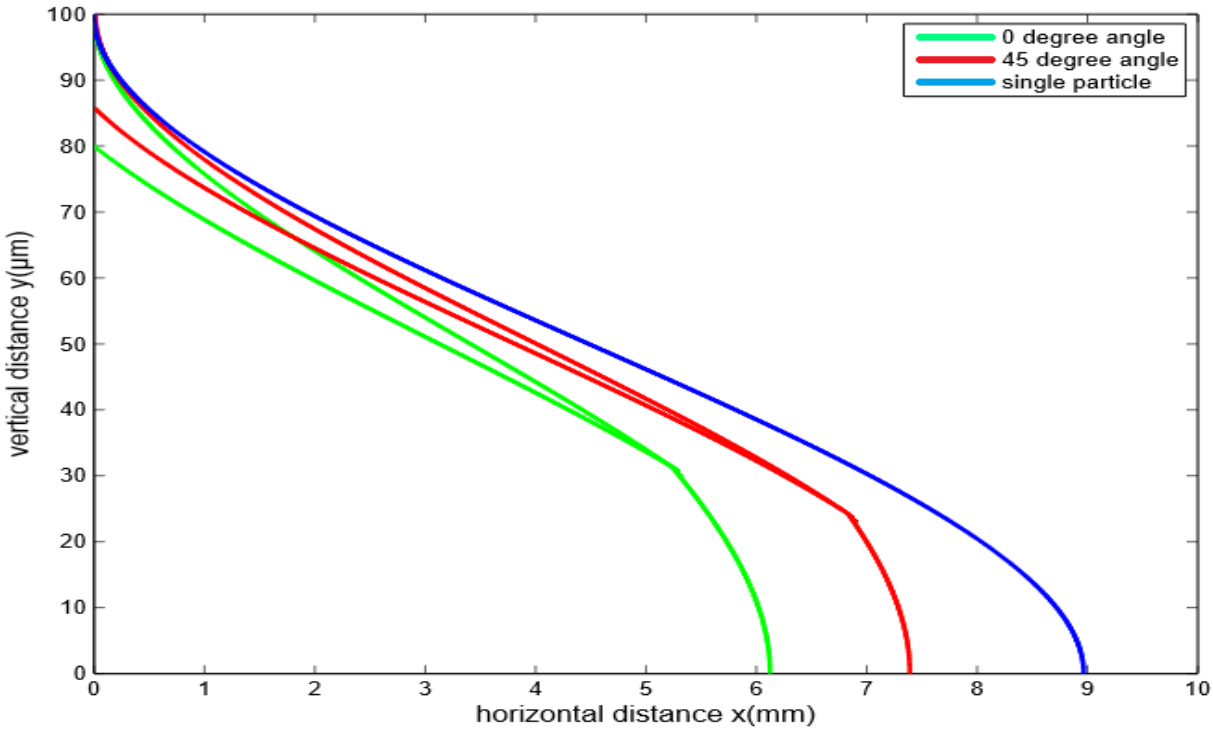

Figure 26: Comparison of trajectories of two cell-bead particle complexes with a single particle trajectory for cases where connector vector is in parallel (0 degree) and at an angle (45 degree) with the applied magnetic field. The distance between particle complexes is twice that of the particle diameter (r=2D).

Comparison of a single particle trajectory with literature

Figure 27 shows a comparison between the trajectory of a single particle trajectory that was performed in this study and a similar study performed by Darabi and Guo[19]. In the present work a fourth order Runge-Kutta method was used to obtain the particle trajectories inside the channel while a first order Euler's method was by Darabi and Guo[19]. Since the Runge-Kutta method is a more accurate integration method, the trajectories obtained from these simulations are more precise than the literature one. The comparison is made for the same geometric and operating conditions. In both cases, the cell size, bead size, number of beads, channel height, flow rate was 10 µm, 1 µm, 6, 100 µm and 50 mL/hr, respectively. It should be noted that the trapping length obtained using the Runge-Kutta method is approximately 10% less than that of the Euler's method.

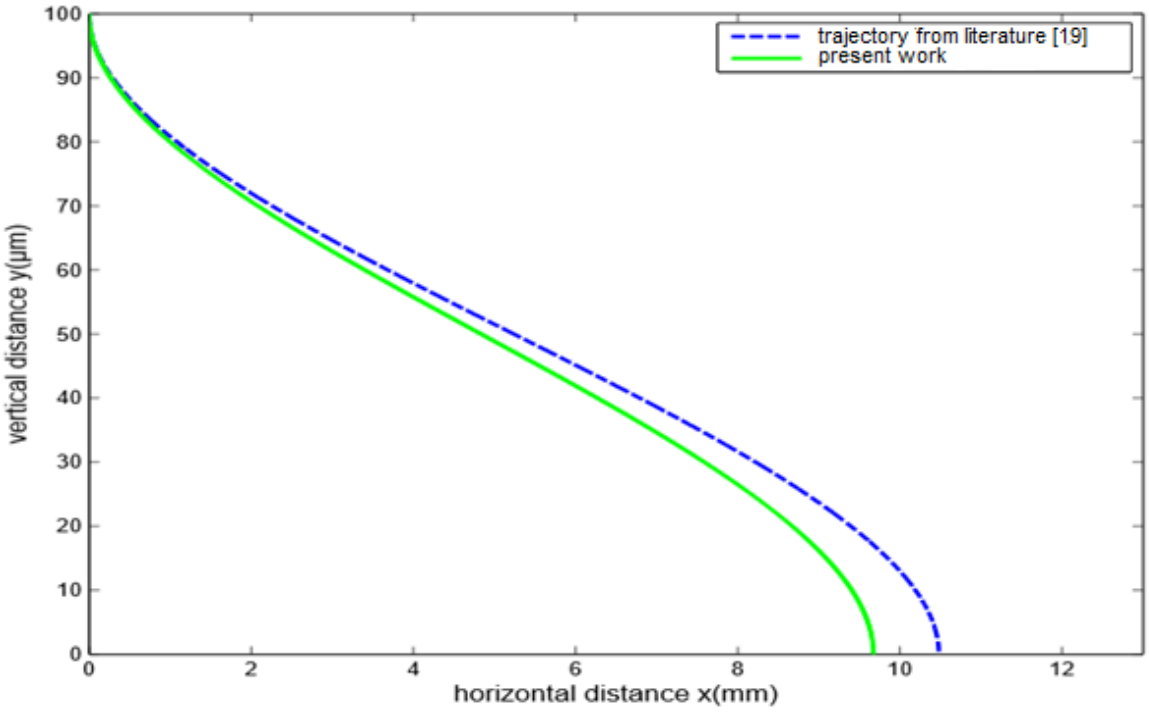

Figure 27: Comparison of a single particle trajectory with the literature. For both cases, the cell size, bead size, number of beads, channel height, flow rate is 10 µm, 1 µm, 6, 100 µm 50 mL/hr, respectively.

Conclusion

This chapter discussed the simulation and analysis of particle interactions and trajectories in a bio-separation chip for various cases where the connector vector is parallel (0 degree), at an angle (45 degree), and perpendicular with the applied magnetic field. The effects of various parameters such as flow rate, cell size, and number of beads per cell on particle trajectories and capture length were investigated. It was found, depending on the dipole alignment with the inter-particle distance, a repulsive or attractive force exerted between particle complexes in the micro-channel.

CHAPTER V

CONCLUSIONS

Introduction

In this thesis, a Lagrangian transport analysis has been performed to predict dipole-dipole interaction between particle complexes in a magnetophoretic bio-separation chip. A theoretical model has been employed to calculate the particle-particle interaction and obtain particle motion trajectories in a microchannel. The basic information about microfluidic bio-separation was provided in Chapter 1. A brief overview of biomaterials, magnetic particles, particle complexes, and interaction between particle complexes were also given in this chapter. Chapter 2 discussed the theoretical framework of the particle tracking inside the channel. In chapter 3, simulations and modelling of particle motion were presented. In chapter 5, the results and discussion of the simulations were provided. Different parametric studies have also been performed to analyze the effect of particle-particle interaction on particle trajectories in the bio-separation chip.

Dipole-dipole interaction

In this work, particle-particle interaction between cell-beads complexes have been performed assuming they can be treated as point magnetic dipoles. In magnetic bio-separation technique, the interaction can be two types. They are dipole-dipole interaction and hydrodynamic interaction. As the particle transport were mainly governed by the magnetic force exerted on the particle, the dominant interaction in this analysis was dipole-dipole interaction. Hence, the hydrodynamic interaction force between particle complexes was neglected for the entire work. Depending on the geometric position and applied magnetic field, the dipole-dipole interaction

force equation was simplified. The geometric positions of the particle complexes were parallel, perpendicular and at 45 degrees with the applied magnetic field. The key findings of the simulations were attractive and repulsive force between complexes depending on the position of magnetic moment to the connector vector distance. When the applied magnetic field were parallel to the connector vector distance, an attractive force between complexes were observed and the interaction force between the particles was repulsive when the magnetic field was kept perpendicular to the connector vector distance. It was also noticed that if the magnetic moment was at an angle of 45 degrees to the connector vector distance, a less dominant attractive force occurred between the complexes than the case where the magnetic moment was parallel with the connector vector distance.

Recommendations for future work

While the model presented in this work can be used for pairwise particle interaction in bio-separation chip, the model can be further refined to improve its accuracy. In these simulations, it was assumed that both the magnetic particles and biomaterials were completely spherical in shape, but in reality, the cell-beads complexes are non-spherical. The lengths of the ligands and receptors around the cell were not calculated in the analysis because of the negligible contact distance between cell and bead compare to their sizes. An analysis of translational motion of particle was performed taking cell-bead complex as a rigid body. The rotation of the complexes was ignored. In the future, a comprehensive analysis can be performed by including the effects of rotation under the influence of magnetic field, molecular and structural changes and the two way coupling between particle and fluid.

The microscale experimental work on particle-particle interaction is a complex phenomenon and there are various challenges associated with these types of experiments. Particularly, it is very hard to predict how particles interact with each other inside a microchannel. Due to this reason, simulation studies play a vital role to understand and optimize such occurrences. After a comprehensive simulation work, sufficient knowledge can be gathered to create a foundation for experimental studies at microscale.

REFERENCES

[1] J. D. Adams, U. kim, H.T. Soh, "High throughput, multi-target magnetophoretic separation," Twelfth International Conference on Miniaturized Systems for Chemistry and Life Sciences, 1302-1304 (2008).

[2] A. Sinha, R. Ganguly, K.D. Anindya, K.P. Ishwar, "Single magnetic particle dynamics in a microchannel", Phys. Fluids, **19**, 117102 (2007).

[3] N. Pamme, "On-chip bioanalysis with magnetic particles,"Curr. Opin, Chem, Biol, **16**, 436-443(2012).

[4] E.P. Furlani, Y. Sahoo, K.C. Ng, J.C. Wortman, and T.E. Monk, "A model for predicting magnetic particles capture in a microfluidic bioseparator," Biomed, Microdevices, **9**,451-463(2007).

[5] O. Philippova, A. Barabanova, V. Molchanov, A. Khokhlov, "Magnetic polymer beads: Recent trends and developments in synthetic design and applications," Europ. Poly. Journal, **47**, 542–559(2011).

[6] S.A. Khashan, E. Elnajjar, Y. Haik, "Numerical simulation of the continuous bio magnetic separation in a two-dimensional channel" Int. J. Multiphase Flow, **37**, 947-955(2011).

[7] A. Radbruch, B. Mechtold, A. Thiel, S. Miltenyi, and E. Pfluger, "Highgradient magnetic cell sorting," Methods Cell Biol, **42**, 387 (1994).

[8] J. Ugelstad, P. Stenstad, L. Kilaas, W. S. Prestvik, R. Herje, A. Berge, and E. Hornes, "Monodisperse magnetic polymer particles—new biochemical and biomedical applications," Blood Purif, **11**, 349 (1993).

[9] P. K. Panigrahi, Transport phenomena in microfluidic systems, J. Wiley & Sons Inc.,Singapore, 284-285(2016).

[10] N. Pamme, C. Wilhelm, "Continuous sorting of magnetic cells via on-chip free-flow magnetophoresis", Lab chip, **6**, 974-980, (2006).

[11] A. A. S. Bhagat, H. Bow, H. W. Hou, S.J. Tan, J. Han, C.T. Lim, "Microfluidics for cell separation", Med. Biol. Eng. Comp., **48**, 999-1014(2010).

[12] A. Bahadorimehr, J. Alvankarian, B. Y. Majlis, Magnetic Force on a Magnetic Bead. ICSE2012 Proc. Kuala Lumpur, Malaysia, (2012).

[13] M. Zborowski, C.B. Fuh, R. Green, L. Sun, J.J. Chalmers, Anal. Chem, **67**, 3702 (1995).

[14] K Nandy, S Chaudhuri, R Ganguly, I K. Puri. Analytical model for the magnetophoretic capture of magnetic microspheres in microfluidic devices. Journal of Magnetism and Magnetic Materials, **320**, 1398–1405 (2008).

[15] J. Darabi, C. Guo, "On-chip magnetophoretic isolation of CD4+ T cells from blood", Biomicrofluidics, **7**, 054106 (2013).

[16] C. Hale, J. Darabi, "Magnetophoretic-based microfluidics device for DNA isolation", Biomicrofluidics, **8**, 044118 (2014).

[17] Sergey S. Shevkoplyas, Adam C. Siegel, Robert M. Westervelt, Mara G. Prentissc and George M. Whitesides. The force acting on a superparamagnetic bead due to an applied magnetic field. The Royal Society of Chemistry 2007, Lab Chip, **7**, 1294–1302 (2007).

[18] J Zhu, L Liang, X Xuan. On-chip manipulation of nonmagnetic particles in paramagnetic solutions using embedded permanent magnets. Microfluidics and Nanofluidics, **12**, 65-73 (2007).

[19] H.-J. Bohm, G. Schneider, "Protein-Ligand Interactions: From molecular recognition to drug design", Wiley-vch GmbH & Co. KGaA (2003).

[20] K. Futosi, S. Fodor, A. Mocsai, Neutrophil cell surface receptors and their intracellular signal transduction pathways, International Immunopharmacology, **17**, 638-650 (2013).

[21] E. B. Pasquale, Eph receptors and ephrins in cancer: bidirectional signaling and beyond, Nat Reviews Cancer, **10**, 165-180 (2010).

[22] H. F. Guo, C. W. V. Kooi, Neuropilin functions as an essential cell surface receptor, The

Journal of Biol. Chem., **290**, 29120-29126 (2015).

[23] I. Safarýk, M. Safarýkova, Scientific and Clinical Applications of Magnetic Carriers, ed. by U. Hafeli, W. Schutt, J. Teller, M. Zborowski ,Plenum, New York, 323 (1997).

[24] C.I. Mikelsen, "Magnetic Separation and hydrodynamic interaction in microfluidic systems", Denmark (2005).

[25] R. Folkersmaa, H.N. Steina, F.N. Vosse, Hydrodynamic interactions between two identical spheres held ®xed side by side against a uniform stream directed perpendicular to the line connecting the spheres' centres, Int. J. of Multi. Flow, **26**, 877-887 (2000).

[26] E. E. Keaveny, M. R. Maxey, "Modelling the magnetic interactions between paramagnetic beads in magnetorheological fluids", Journal of Computational Physics, **227**, 9554-9571.

[27] D. Du, D. Li, M. Thakur, S. Biswal, "Generating an in situ tunable interaction potential for probing 2-D colloidal phase behavior", Soft Matter, **9**, 6867-6875 (2013).

[28] N. Osterman, I. Poberaj, J. Dobnikar, D. Frenkel, P. Ziherl, D. Babić, "Field-Induced Self-Assembly of Suspended Colloidal Membranes", Phys. Rev. Lett.,**103**, 22-27 (2009).

[29] U. Jeong, X. W. Teng, Y. Wang, H. Yang, Y. N. Xia, 2007, Adv. Materials, "Superparamagnetic colloids: controlled synthesis and niche applications",**19**, 33-60.

[30] P. Tierno, O. Guell, F. Sagues, R. Golestanian, and I. Pagonabar-raga, 2010, "Controlled propulsion in viscous fluids of magnetically actuated colloidal doublets", Phys. Rev. E, 81, 011402.

[31] Yang Gao, Alexander van Reenen, Martien A. Hulsen, Arthur M. de Jong, Menno W. J. Prins and Jaap M. J. den Toonder,"Disaggregation of microparticle clusters by induced magnetic dipole–dipole repulsion near a surface", Lab Chip, **13**, 1394-1401(2013).

[32] E. Climent, M. Maxey, G. Karniadakis, "Dynamics of self-assembled chaining in magnetorheological fluids", Langmuir, **20**(2), 507-513.

[33] E.E. Keaveny, M.R. Maxey, "Modeling the magnetic interactions between paramagnetic beads in magnetorheological fluids", J. Computational Physics, **227(22)**, 9554- 9571(2008).

[34] S. Melle, O. Calderon, M. Rubio, G. Fuller, "Microstructure evolution in magnetorheological suspensions governed by Mason number, Phys. Rev. E, **68**, 041503(2003).

[35] J. Greene, F.G. Karioris, "Force on a magnetic dipole", American J. Physics, **39**, 172-175(1970).

[36] T.H. Boyer, "The force on a magnetic dipole", American J. Physics, **56**, 688-692 (1988).

[37] P. Hrasko, "Forces acting on magnetic dipoles", II Nuovo Cimento 3B, 213-224.

[38] K. R. Brownstein, "Force exerted on a magnetic dipole", American J. Physics, **61**, 940-941 (1988).

[39] L. Vaidman, "Torque and force on a magnetic dipole", American J. Physics, **58**, 978-983 (1990).

[40] K. W. Yung, P. B. Landecker, D. D. Villani, "An analytic solution for the force between two magnetic dipoles", Magnetic and Electrical Separation, **9**, 39-52.

[41] S.A. Khashan, A.Alazzam, E.P. Furlani, "Computational Analysis of Enhanced Magnetic Bio-separation in Microfluidic Systems with Flow-Invasive Magnetic Elements", Sci. Rep., **4**, 5299 (2014).

[42] Mark M. Clark, "Transport Modeling for Environmental Engineers and Scientists", A John Wiley & Sons Inc., New Jersey, 37-38.